2007

Fabrication and Analysis of Poly(3-hexylthiophene) Interfaces Using Electrospray Deposition and Photoemission Spectroscopy

John Lyon
University of South Florida

Fabrication and Analysis of Poly(3-hexylthiophene) Interfaces Using Electrospray Deposition and Photoemission Spectroscopy

By

James Lyon

A thesis submitted in partial fulfillment
of the requirements for the degree of
Master of Science in Electrical Engineering
Department of Electrical Engineering
College of Engineering
University of South Florida

Major Professor: Rudy Schlaf, Ph.D.
Matthias Batzill, Ph.D.
Hua Cao, Ph.D.

Date of Approval:
April 5, 2007

Keywords: XPS, UPS, P3HT, electronic structure, orbital lineup

Dedication

To Dr. Schlaf for giving me the opportunity to engage in research at the undergraduate level and for inspiring me to pursue a graduate degree.

Acknowledgements

I would like to thank Dr. Rudy Schlaf for allowing me the opportunity to engage in research, Dr. Martin Beerbom and Dr. Yeonjin Yi for their advice and instruction, and my family for their constant support. Financial support from the National Science Foundation and the College of Engineering REU program is gratefully acknowledged.

Table of Contents

List of Figures

Fabrication and Analysis of Poly(3-hexylthiophene) Interfaces Using Electrospray Deposition and Photoemission Spectroscopy

James Lyon

ABSTRACT

P3HT (Poly(3-hexylthiophene)) is an organic polymer that shows promise as an active material in semiconducting electronics. It is important to study the electronic properties of this material in order to determine its efficacy in such devices. However, many current studies of thiophene only examine the oligomer, since it is a simpler material to investigate.

In this study, several P3HT interfaces were analyzed to determine their electronic properties. The P3HT was deposited on Au, highly-ordered pyrolitic graphite (HOPG), and indium tin oxide (ITO) substrates via electrospray deposition. The depositions were performed in several steps, with x-ray photoemission spectroscopy (XPS) and ultraviolet photoemission spectroscopy (UPS) measurements taken between each step without breaking the vacuum. The resulting series of spectra allowed orbital line-up diagrams to be generated for each interface, giving detailed analysis of the interfacial properties, including the charge injection barriers and interface dipoles. The results, when compared to similar oligomer-based investigations, show a difference in the orbital line-up between oligomeric and polymeric P3HT junctions.

Introduction

The last decade has seen increased interest in the fabrication of polymer electronics. Organic/inorganic interfaces have promising potential application in so-called "plastic electronics," thanks to their material properties and low cost. The conjugated polymer poly(3-hexylthiophene) (P3HT) is a promising organic material for these devices, due to its relatively high drift mobility and semiconducting properties. Recent devices utilizing P3HT interfaces include organic solar cells [1, 2] and field-effect transistors [3, 4].

Electronic devices typically rely on material interfaces for operation. These interfaces create an asymmetric junction which drives current in a particular direction. Different materials create interfaces with differing properties. It is necessary to investigate the properties of these junctions to determine which materials are optimal for a particular device. These investigations are frequently performed using Photoemission Spectroscopy.

Photoemission spectroscopy (PES), which includes x-ray PES (XPS) and ultraviolet PES (UPS), is a surface science technique that provides information about the surface of a sample. XPS shows the chemical interactions of the interface and of the individual molecules themselves, while UPS allows determination of the many of the interface properties, including charge injection barriers and interface dipoles. It is a surface sensitive technique and is not sensitive to the bulk of the substrate, thus giving a

view only of the surface and the newly created interface. Its high surface sensitivity requires performance of the measurements in UHV to avoid contamination issues.

Interfacial investigations using PES were first carried out by Waldrop and Grant on inorganic interfaces [5]. As organic materials began to be considered for use in electronic devices, this method was expanded to organic interfaces, such as polymer/metal junctions [6].

Polymeric interfaces, including ones utilizing P3HT, are difficult to fabricate, mainly due to the fragility of the polymers. Evaporation of the polymer in vacuum is ruled out because of the high molecular weight of polymers, making them nonvolatile even at high temperatures. Many investigators have taken to creating polymeric films ex-situ through the use of spin coating. Such a process was carried out by Salaneck et al. in their investigation of organic-metal interfaces via UPS [6], and by Atreya et al. in a similar study that examined the interactions between evaporated metals and the polymer MEH-PPV [7]. Ex-situ creation of polymeric films, however, exposes the polymeric substrate to ambient conditions, introducing environmental contaminants. Evaporation of metal onto a polymeric substrate in-vacuum is a possibility, but the evaporated, highly-energetic metals atoms may damage the polymer film. To allow for in-situ evaporation of organic materials for interfacial investigations, some researchers substituted the oligomer for the polymer when investigating the properties of organic interfaces, basing their actions on the apparent similarities between the oligomers and polymers of organic materials. Oligomers have a lower molecular weight than their polymeric counterparts, and as such are easier to evaporate. However, assumptions about the similarities between oligomers and polymers may create challenges in the interpretation of the nature of the

polymeric junctions. Fujimoto et al. and Chandekar and Whitten have both investigated the differences in electronic structure between short and long-chain oligomer films [8, 9]. Other researchers have focused on other non-vacuum techniques to investigate these interfaces, such as I/V curves.

Electrospray thin film deposition is a fabrication process that eliminates these preparatory constraints. Electrospray allows the direct injection of macromolecules from solution into high vacuum. It has been primarily used in the past to introduce large molecules into mass spectrometry devices, and has only recently been considered for thin film deposition in vacuum [10-12]. The injected polymers can be deposited on various substrates in several steps without breaking the vacuum and without damage to the polymer. This multi-step deposition process permits x-ray photoemission spectroscopy (XPS) and ultraviolet photoemission spectroscopy (UPS) measurements in between deposition steps. The thin films produced by electrospray deposition allow XPS and UPS to clearly characterize the resulting interface.

Several previous investigations of P3HT interfaces examined only the finished interface, without examining its properties as it was grown [6, 7]. The studies presented here, in contrast, use the multi-step deposition technique in which the interface was analyzed at each step of deposition, allowing a detailed characterization of the junction during its formation. Clean samples were exposed to the deposition process and then sent in-situ to an analysis chamber, where PES was performed. The process was then repeated several times, each deposition step longer than the previous one.

This multi-step process allowed evaluation of the electronic interface, detection of charging and other measurement-related phenomenon, and a view of the subtle growth of

interface characteristics such as band bending. The combination of electrospray deposition to grow actual polymeric interfaces, the multi-step deposition process, and in-situ characterization makes these sets of experiments unique in their ability to probe the exact details of the growth of these interfaces and their precise device characteristics.

Materials

Au (gold) is a transition metal element, so called because of its partially filled d-sub-shell. D-orbital electrons have a high likelihood of delocalizing within the metal lattice, and this gives gold and other transition metals a number of properties, such as high tensile strength, density, melting and boiling points, and its characteristic color. Because of its high conductivity and resistance to corrosion, gold is frequently used as electrical contacts for various solid state devices.

As a solid, gold forms a continuum of energy levels to create a valence band, as with other solids. The d-bands of gold contain more energy levels than its s and p orbitals within a narrower range [13]. This leads to high electron density levels at the energy levels where the d-bands lie, and consequently high, sharp peaks in gold's valence band energy spectra. This feature can be clearly seen in Figure 19. The large peaks in the gold sample's valence band correspond to density spikes from the element's d-bands.

Most metals possess a cloud of electron gas about their surface, creating a dipole that increases the work function of the metal [14]. When an organic material is deposited onto the metal, the cloud of electrons is "pushed back" into the surface of the metal, reducing the work function. It is the pushing back of the electronic cloud which results in the large interface dipoles found between gold and P3HT in this experiment.

HOPG

HOPG (highly ordered pyrolitic graphite) is one of the allotropes of carbon. It consists of sheets of hexagonally ordered carbons. HOPG has a relatively high electrical conductivity compared to diamond. This is due to the presence of delocalized pi orbital electrons across the hexagonal lattices of the graphite sheets. The hybridized sp2 orbitals form covalent bonds between the carbon atoms within a single sheet, while the sheets are held together by much weaker van der Waals forces, making layers easy to shear off one another and permitting the cleaving of HOPG sample in situ to achieve a contamination-free surface.

Partially due to its lack of d-orbital electrons, HOPG has relatively weak valence band emissions. This makes it an ideal substrate for investigating the formation of P3HT valence band emissions as the P3HT is deposited. The HOMO cutoff position of P3HT is more easily seen on HOPG substrates. Consequently, a more accurate P3HT ionization energy can be obtained, which can be used for the evaluation of experiments on more challenging substrates

HOPG creates only weak interface dipoles with organic materials, due to the lack of primary bonding between the HOPG and the polymer. The organic material adheres to the HOPG only through van der Waals forces, circumventing the usual processes for creating dipoles.

ITO

Indium Tin Oxide (In_2O_3:Sn or ITO) is a mixture of indium oxide and tin oxide. Transparent and colorless, its high electrical conductivity makes it an ideal electrode for many devices, especially the transparent layer of solar cells.

Since ITO is a degenerately n-doped material [15], its Fermi level can be expected to lie within the conduction band, and not in the bandgap, as found in moderately doped semiconductors. However, the surface of the ITO contains a higher concentration of oxygen, due to the ITO's treatment in ambient conditions. This excess of oxygen reduces the degeneration of the ITO, lowering its Fermi level to inside the band gap and thus increasing its work function. The high work function of such an ITO sample makes it a promising anode for electronic devices. Figure 1 shows a comparison between ITO films with a 0% and 10% oxygen content.

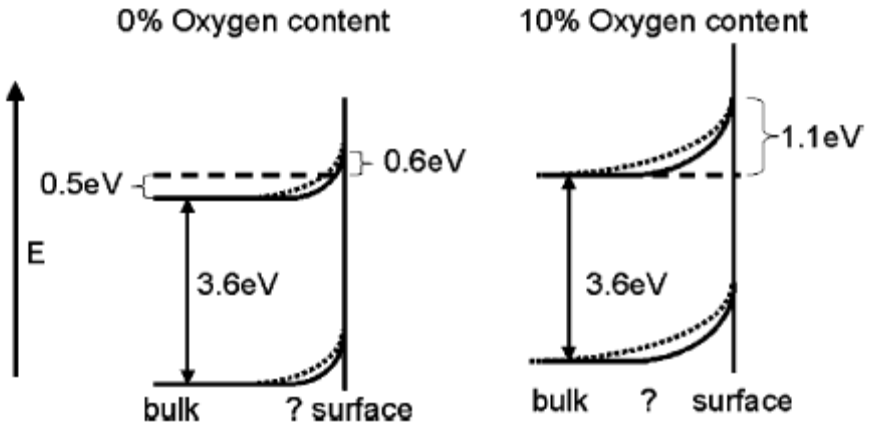

Figure 1: Band Diagram for Two ITO Films With Differing Oxygen Contents (from Reference [15])

Polythiophene

Polythiophene is an organic semiconducting polymer. Semiconducting polymers are a relatively recent phenomenon, having been discovered at the end of the 1970's by Heeger and MacDiarmid, who synthesized a polyacetylene chain with a 12 orders of magnitude increase in conductivity upon charge-transfer oxidative doping [16]. Their conductivity is highly anisotropic, mainly along the chain of the polymer. Work on

conducting polymers (CP) began to accelerate, with many new suitable organic materials researched. Researchers were interested in CP because of their advantages over traditional semiconducting materials: low cost, ease of processing, light weight, and resistance to corrosion.

Thiophene is an aromatic, heterocyclic compound. The non carbon element in the compound is sulfur, which forms one node of a ring of alternating single and double bonds with four atoms of carbon. The single bonds are formed by sigma bonding between electrons in the plane of the carbon nuclei. The double bonds are formed via a sigma bond and a pi bond formed by an overlap of p-orbitals above and below the plane of the ring. These orbitals, since they are out of the plane of the nuclei, are free to interact and move as they wish, and hence become delocalized. In addition to these electrons in the pi bonds, the lone electron pairs on the sulfur atom also participate significantly, giving thiophene a high charge mobility and its semiconducting properties. This type of system is known as a conjugate system: the single and double bonds delocalize the pi electrons to lower the overall energy of the molecule and increase stability. Figure 2 displays a diagram of a P3HT molecule.

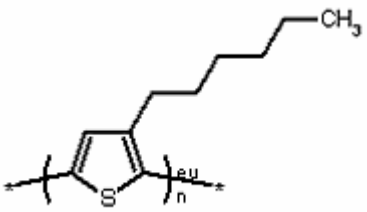

Figure 2: Diagram of a Monomer in a Poly(3-hexylthiophene) Chain (from Reference [16])

Interfaces

Metal-Metal Interfaces

In a metal, energy states are filled to the Fermi level of the sample, there is a charge transfer that occurs from the lower work function metal to the higher work function. Figure 3 shows two metals before and after contact. This happens because the electrons in the lower work function metal possess a higher energy than those in the lower work function metal. Upon contact, the lower work function's electron tunnel over to the lower available energy states in the higher work function metal. This electron transfer reduces the total energy of the dual system, but at the same time negatively the higher work function metal with regard to the lower work function metal. This charge imbalance creates a contact voltage (or potential difference) between the two metals [14].

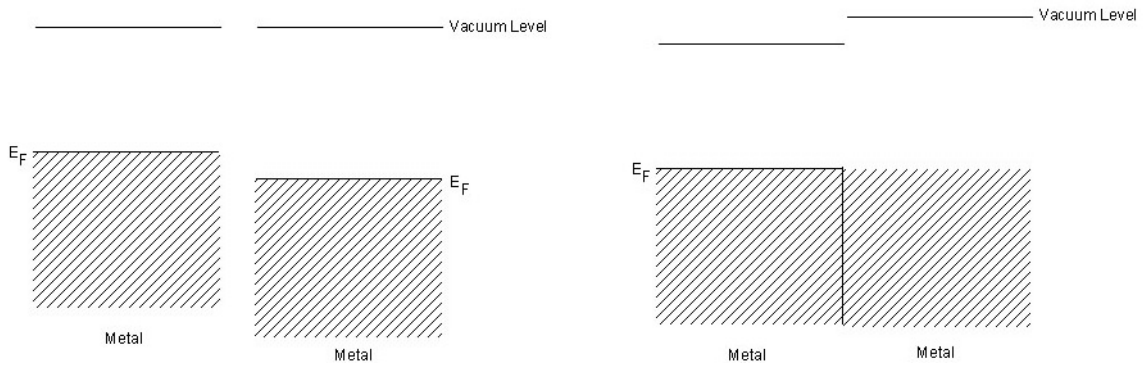

Figure 3: Two Metals Before and After Contact

Metal-Semiconductor Interfaces: Schottky Barriers

When a metal and a semiconductor are brought into contact, there is the possibility of the formation of a Schottky barrier. A Schottky barrier is an interface with rectifying properties; that is, charge is able to flow easily in one direction, but is impeded when attempting to flow in the other direction. Figure 4 shows a metal and semiconductor before and after contact.

In the Schottky barrier model, we assume that $\Phi_m > \Phi_n$, the work function of the smaller is greater than that of a p-type semiconductor (the doping type of P3HT). This impels the holes in the VB of the semiconductor to tunnel to the higher energy states available in the metal. This creates a contact (built-in) potential, as with metal-metal contacts. This potential eventually becomes strong until to impede the further flow of charge, and the Fermi levels within the materials equilibrate. This charge transfer creates a depletion region in the semiconductor near to the metal. Since this region has been depleted of charge carriers, it constitutes a space charge layer (SCL), or a non-uniform internal field directed away from the surface of the metal. This space charge layer causes the bands of the semiconductor to bend, because the charges within the semiconductor are not free to move and redistribute the charge to keep the bands in the SC flat. Figure 4 shows a typical metal-semiconductor contact. The PE barrier for charge moving from the metal to the semiconductor is known as the Schottky barrier height Φ_b. When the junction is biased so that the metal is connected to the negative terminal and the semiconductor is connected to the positive terminal, a voltage drop occurs at the depletion region. This causes the bands of the semiconductor to shift downwards, while keeping Φ_b the same. The decrease in the steepness of the VB permits holes to overcome the potential barrier and move to the metal, creating a current.

Reversing the bias causes the SC bands to shift further upward. The holes in the metal cannot overcome the Schottky barrier height to reach the SC, and so no current flows.

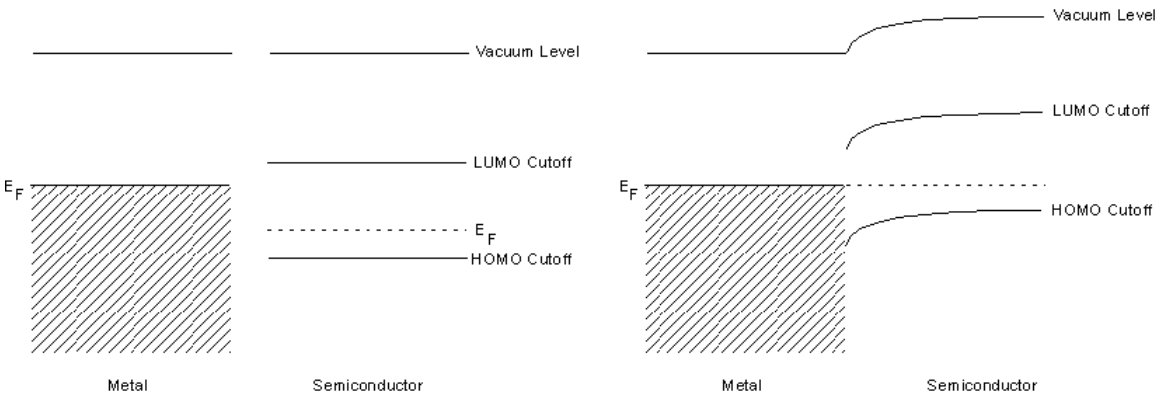

Figure 4: A Metal and a Semiconductor Before and After Contact

Interface Dipoles

In both metal-metal and metal-semiconductor interfaces, a common vacuum level (VL) is usually assumed. However, this is generally not the case for most metal-organic contacts. Generally, a surface dipole exists at the interface between the metal and the organic material [14].

Around the surface of a metal, the electrons are free enough to form an "electron cloud." This creates a surface dipole, since the area around the metal has become negatively charged by the electron cloud, and the consequent lack of electrons inside the surface makes the bulk side positive. When a molecule comes into contact with the metal, a dipole forms between the two materials. This can be due to interfacial charge transfer, redistribution of the metal's electron cloud, an interfacial chemical reaction, and other

localized charge rearrangements. The pushing of the metal's electrons back into its surface reduces the free metal dipole, thus reducing the work function of the metal at the interface. This is displayed as an asymmetry in the vacuum level between the metal and the organic layer. Figure 5 shows the formation of a dipole between a metal and an organic layer after contact, while Figure 6 shows the various ways such a dipole could form.

Such interface dipoles are important to consider when investigating the properties of an interface, as they have strong repercussions on the properties of the junction. A misalignment of the vacuum level between the metal and the organic material reduces the band bending at the organic material's surface, changing the injection barriers of the interface and thus altering the interface's performance when used in electronic devices. Figure 7 shows a comparison of a metal-organic junction with and without an interfacial dipole, comparing the effects of the dipole on its band structure.

Metal-Polymer Interfaces

Polymeric materials differ in their electronic structures from semiconductors. Organic polymers are composed of polymeric chains held together by weak van der Waals attraction. This means that their core atomic orbitals (AOs) are still localized, but their valence levels interact to form delocalized molecular orbitals (MOs). The density of these orbital levels can be fine-grained or more spaced apart, depending on the number of atoms in the polymer chain [14]. The highest MO in an organic polymer is known as the highest occupied molecular orbital, or HOMO, and the lowest energy level in the conduction band is known as the lowest unoccupied molecular orbital, or LUMO.

Electrons in the valence band and lower conduction bands of a polymeric material are localized and can only travel along the path of the one dimensional polymeric chain, whereas those in the higher conduction band levels become delocalized and can freely travel from chain to chain.

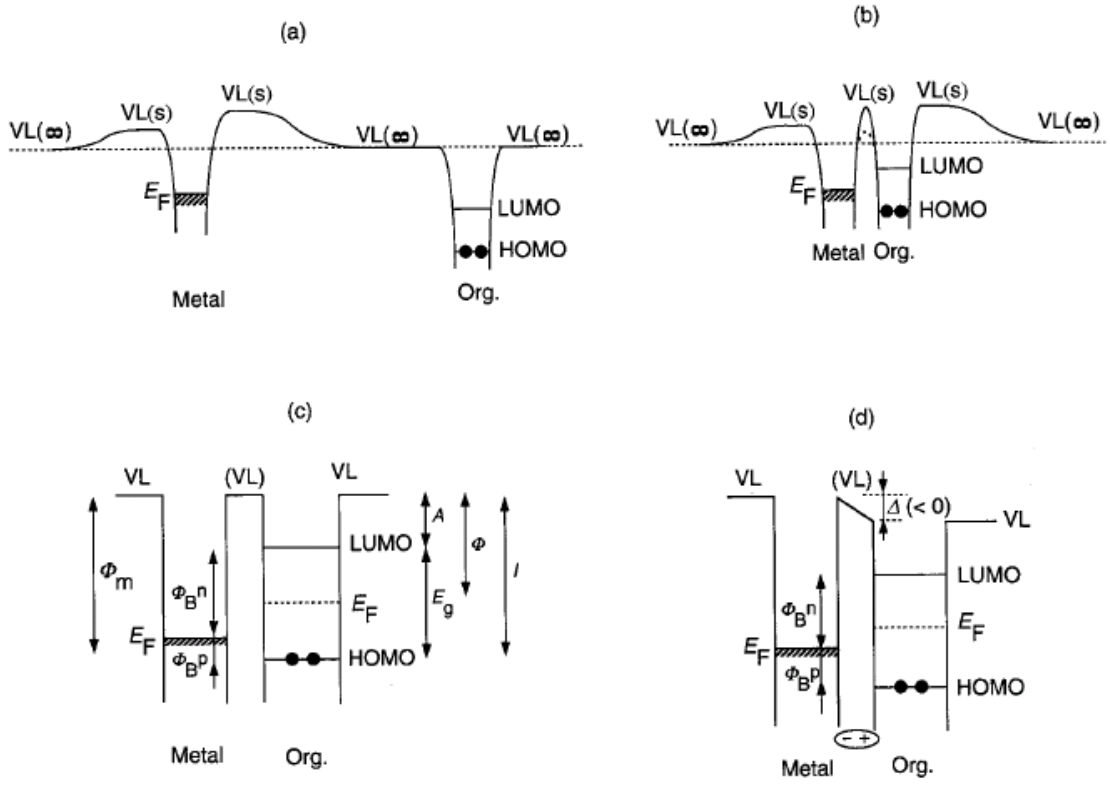

Figure 5: Formation of a Dipole Between a Metal and an Organic Layer(from Reference [14])

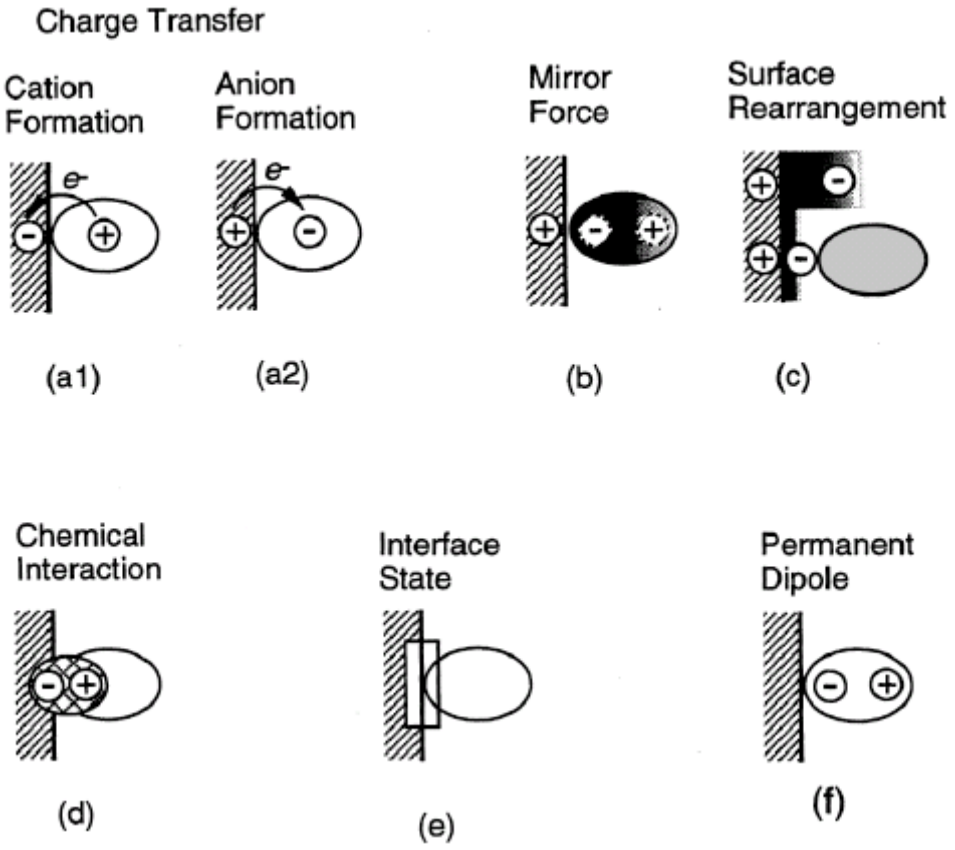

Figure 6: Possible Factors Forming and Affecting Interfacial Dipole Layers (from Reference [14])

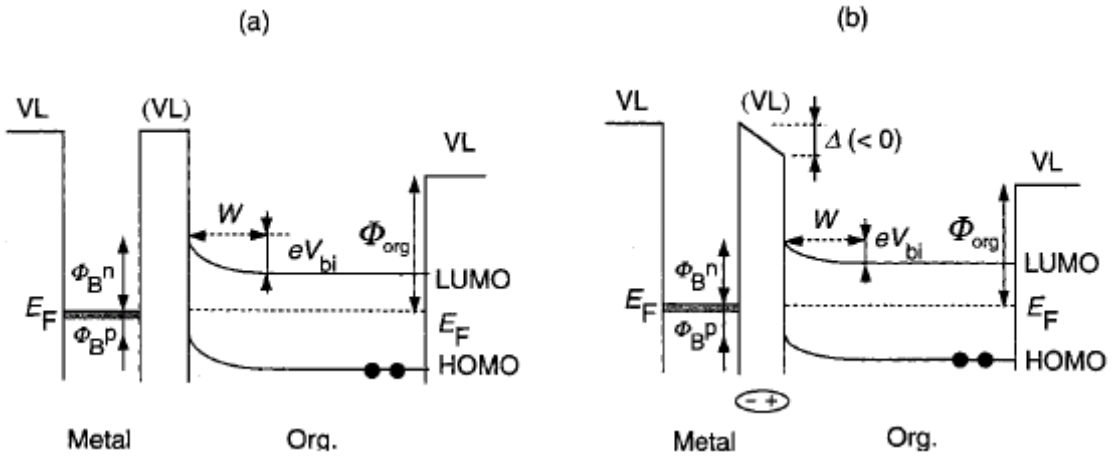

Figure 7: Comparison of a Metal-Organic Interface a) With and b) Without the Shift in Vacuum Level (VL) Corresponding to a Dipole (from Reference [14])

Electrospray

Electrospray is a method which allows direct injection of macromolecules into high vacuum. It is useful for processes such as mass spectrometry and thin film depositions on substrates.

Growing organic thin films can be a challenging process. Organic materials cannot be deposited by evaporation, because their high molecular weight makes them difficult to evaporate, and the fragility of the polymers is increased by the heat. Spin coating is a popular method, but must be done in ambient conditions, exposing the subsequent film to environmental contaminants.

Figure 8 shows a schematic of the Electrospray process. Electrospray works by creating small ionized droplets by application of an external electric field between a capillary and a counter electrode. The charged molecules within the solution move from liquid phase to gas phase during the process, where they are directed for use in a mass spectrometer or for thin film growth. During the process, an inert or nebulizing gas is sometimes used to increase flow rates and permits use of solvents with higher surface tensions.

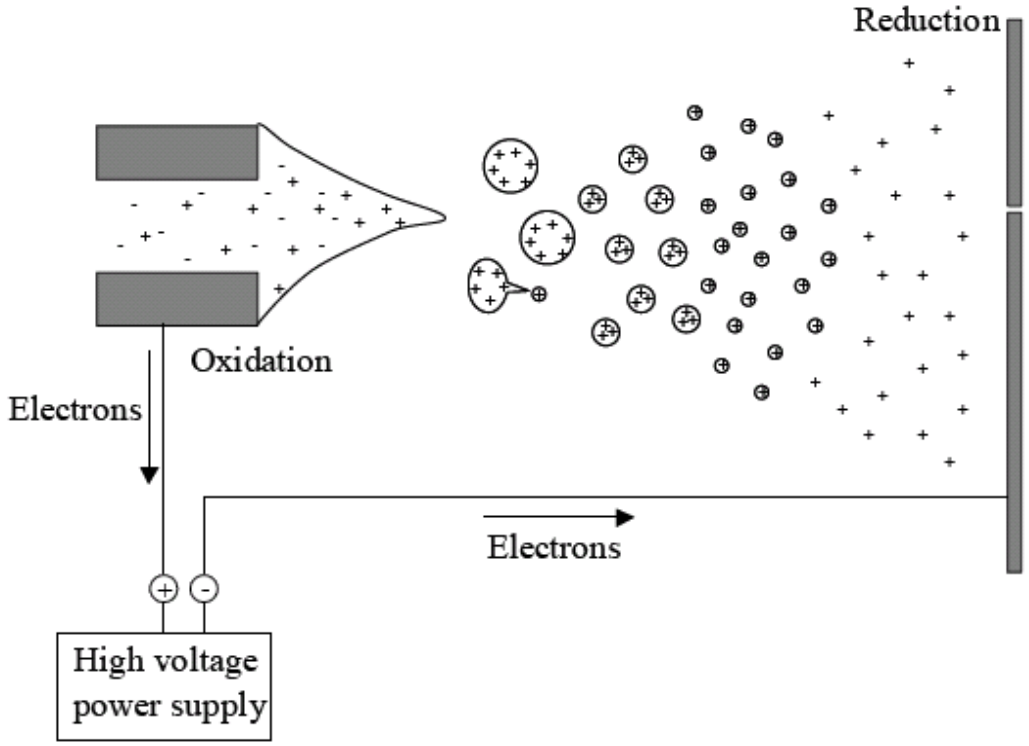

Figure 8: Process of Electrospray Deposition Technique (from Reference [17])

Historical Background

The first known reference to the electrospray phenomenon was by W. Gilbert in the year 1600, in his book "De Magnete," where he discussed the most recent discoveries in the then nascent fields of electricity and magnetism [18]. Nearly 200 years later, G.M. Bose [19] and L'abbe J. – A. Nollet [20] both noted a possible existence of electrospray in their experiments, the former while applying electric potential to a glass capillary and the latter while experimenting with human blood and electricity.

Until the 1960's, electrospray was mainly utilized as a painting technique, the process being described by Burton and Weigand. During the 1960's, the Taylor cone was first discovered by Sir Geoffrey Ingram Taylor [21]. In the 1980's, the groups of

Fenn [22, 23] and Alexandrov [24] independently used electrospray to generate gas phase ions for mass spectrometry successfully for the first time. In 1987, Bruins et al. used a process known as pneumatically assisted electrospray, or Ionspray, which first used a nebulizing, inert gas to assist in charge aerosol formation [25]. In 1988, Fenn et al. [26] achieved multiple charging, making it possible to analyze large molecules on mass spec machines with limited mass range, and greatly increasing interest in electrospray. A technique called Nanospray was developed by Wilm and Mann in the mid 1990's to generate electrospray using low flow rates (nl min^{-1}) [27].

Physical Basis

The process of ESI can be broken down into three steps:

1. Charge droplet formation at the capillary tip.

   The charge is induced by an external applied electric field between the capillary tip and a counter electrode. Charge separation occurs, the charge depending on the bias of the capillary, and if the field is strong enough, a Taylor cone will develop and protrude from the capillary, as well as a thin liquid jet, where small, charged droplets are generated in a fine mist.

   During the charge droplet formation stage the Taylor cone can be observed. This cone is created by the rearrangement of charge produced by the external field. If the solution is conductive enough, the solution's cations will (in positive mode) move towards the field's strongest point, the tip of the capillary, while the anions will migrate away from the surface. The counteracting of this electric force with the surface tension of the liquid will

create a cone (the Taylor cone) at the capillary tip. When the external potential becomes high enough, a liquid jet will emerge from the cone, ejecting charged droplets. The potential needed to generate a stable electrospray and the subsequent Taylor cone can be generated with this equation [28]:

$$V_{on} = A_1(2\gamma r_c \cos(\theta)/\varepsilon_0)1/2\ln(4d/r_c)$$

Where V_{on} is the electrospray onset voltage (V), A_1 is the dimensionless constant ~0.5-0.7, γ is the surface tension (Nm-1), r_c is the capillary radius (m), θ is the half angle of the Taylor cone apex, ε_0 is the electrical permittivity in vacuum (C2N-1m-2), and d is the spray needle – counter electrode distance (m)

2. Evaporation of solvent from the droplets.

   As the charged droplets are impelled forward by the external field, their radius will decrease as the solvent evaporates and is pumped out by vacuum pumps. At a point known as the Rayleigh limit, the Coulombic forces will overcome the liquid's surface tension and the droplet will undergo fission, separating into several smaller droplets. This process can repeat, creating even smaller and more densely charged droplets.

3. Formation of gas phase ions.

   At a certain point in the electrospray process, the solvated ions transfer to gas phase ions. Two main theories have been proposed for this process: the

charged residue mechanism (CRM) and the ion evaporation mechanism (IEM). It has been suggested that both these processes can occur, but for differing analyte types. The two methods of gas phase ion formation have been debated since the 1960's. The Charged Residue Model (CRM), by Dole et al. [29], reasons that the droplets keep undergoing fission into smaller and smaller droplets until only one macromolecule per drop remained. The evaporation of the rest of the solvent leaves the macromolecule intact and isolated. The Ion Evaporation Model (IEM) by Iribane and Thomson [30] proposed that when the droplets have shrunk to a certain size, the ionic macromolecules would be emitted directly from the droplets.

Photoemission Spectroscopy

Photoemission (or photoelectron) spectroscopy (PES) is an analysis procedure whereby monochromatic photons impinge upon a sample, ionizing electrons. This process of ionization, known as the photoelectric effect, allows a detailed investigation of a material's electronic properties and chemical composition. The emitted electrons have a kinetic energy equal to the energy of the photons minus the energy required to ionize them. The electrons are collected in an analyzer, where a count of the number of electrons with a particular kinetic energy is performed. This produces a spectrum which can be used to characterize a sample.

Two types of PES were used in these experiments: x-ray photoemission spectroscopy (XPS) and ultraviolet photoemission spectroscopy (UPS). The soft x-rays used for XPS are in the 200-2000 eV range and can be used to examine the core energy levels of a sample, while UPS, using narrow line width UV light in the 10-45 eV range, is used to examine the valence bands with high resolution.

Physical Basis

The photoelectric effect was first observed by Alexandre Edmond Becquerel in 1839, by exposing an electrode in a conductive solution to light. Despite this, Heinrich Hertz is generally recognized to be the discoverer of the phenomenon (giving the effect a third, though obsolete nomenclature: The Hertz effect). His experiment consisted of two arcs, a driving and secondary one. The secondary arc was observed to be more

pronounced when it was not shielded from the driving arc by a pane of glass. Substituting the glass shield for a quartz one produced no noticeable difference in the arc. Hertz concluded that ultraviolet light from the driving arc increased the arc length by assisting the electrons in jumping across the gap. The glass pane absorbed the UV and hence reduced the arc length, while the quartz, which does not absorb UV, did not affect it. Hertz made no further effort to explain the results.

It was Einstein who first proposed an explanation of the effect, using the newly formulated rules of quantum mechanics. It was observed that higher intensity light increased the current of the emitted electrons, whereas higher energy did not. Einstein's explanation of the photoelectric effect in 1905 [31] was part of his *annus mirabilis* burst of papers, during which he also revealed special relativity and the equivalence of matter and energy.

When a photon impinges on an electron, it imparts all its energy to the electron (Einstein concluded definitely that a photon is not able to transfer a portion of its energy). If the energy received by the electron is greater than the work function of the material the electron resides in, the electron is ionized and ejected out from the material. The energy of the photon striking the electron is

$$E = h\upsilon \qquad (1.)$$

where E is the energy, h is planck's constant, and υ is the frequency of light. The binding energy, BE, of the electron is the energy required to move an electron from its initial position to the Fermi level of the solid. The Fermi level is located in between the high occupied molecular orbital (HOMO) and the vacuum level. The work function, Φ, of the material is the energy difference between the Fermi level and the vacuum level. When a

photon impinges on an electron, the electron must overcome first its BE and then the material's Φ in order to escape into vacuum. If it manages to ionize, the remaining energy of the photon is considered to be the electron's kinetic energy, KE. Thus,

$$KE = h\upsilon - BE - \Phi \qquad (2.)$$

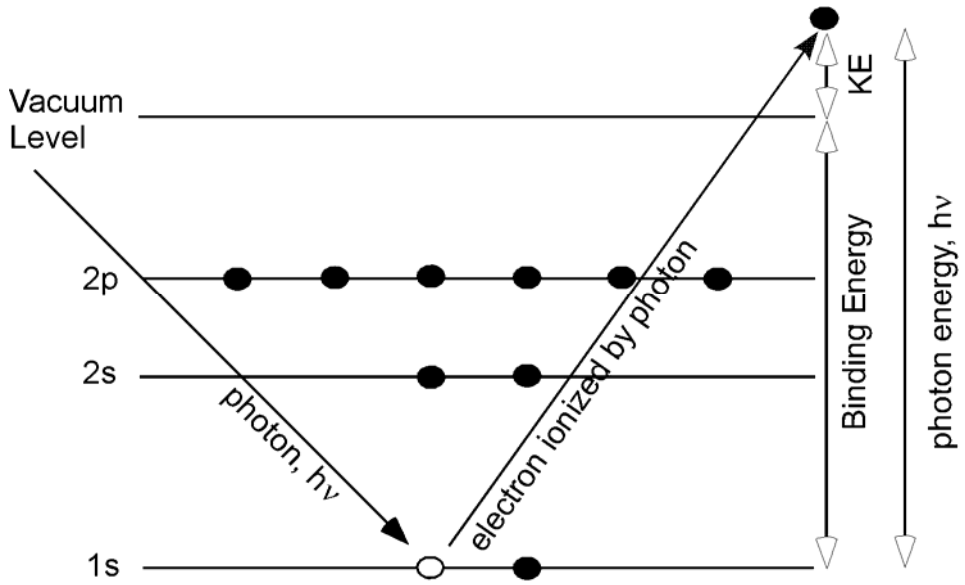

Figure 9: Photoelectric Effect for a Model Atom

Figure 9 shows the photoelectric effect schematically. In this presentation, the work function of the material is included in the binding energy. The loss of the electron produces a positively charged hole is represented by a white circle. The KE of the ionized electron is shown on the right to be the photonic energy after the loss of the energy required to ionize the electron.

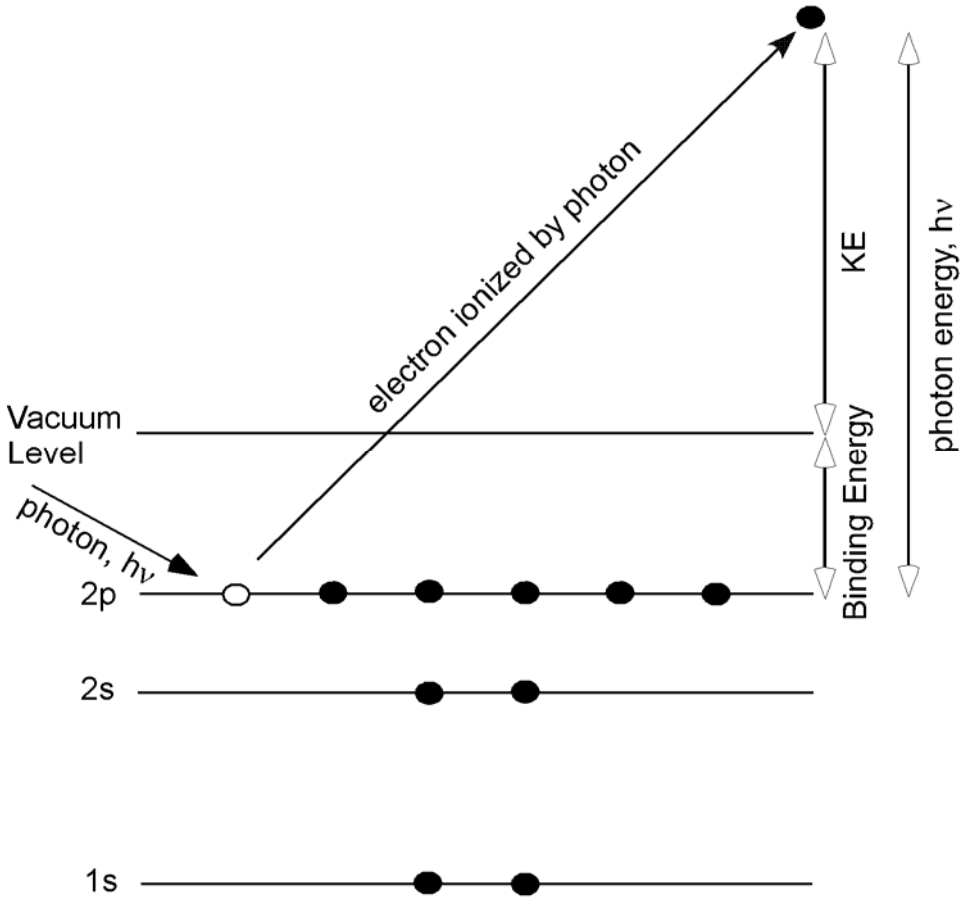

Figure 10: Photoelectric Effect for a Model Atom at 2p Orbital

Figure 10 displays the photon striking a lower BE electron, this one in the 2p orbital. Since the electron has a lower BE, more of the energy of the photon is transformed into the ionized electron KE.

When an electron is emitted from a sample, it leaves a hole behind in its orbital. This hole may be filled by another electron dropping down from a lower BE. The lowering of this secondary electron's energy causes the electron to emit a photon, which in turn may impinge upon another electron and ionize it. This emitted electron is known as an Auger electron. Since the Auger electron receives its energy from another electron, its energy is independent of the original photon energy, and instead depends on the

difference in energy between the secondary electron's BE before and after dropping to a lower orbital.

Figure 11 shows the process of Auger electron creation. Line A shows an electron dropping from its initial state to the orbital of a previously ionized electron. Its release of energy upon dropping has the effect of ionizing a second electron into the vacuum level, line B. Since Auger electrons are referenced by the orbitals involved in the process, the electron would be called a $KL_{23}L_{23}$, or KLL electron.

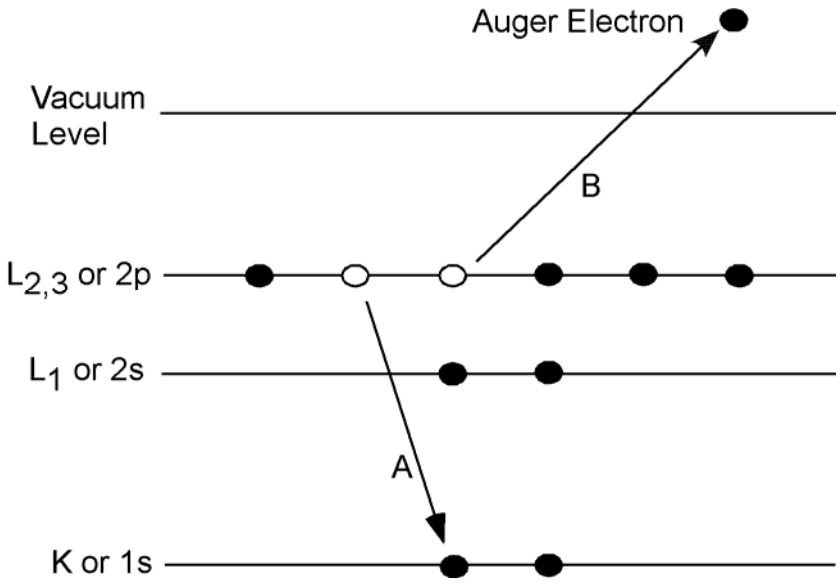

Figure 11: Auger Effect for a Model Atom

PES Equipment

PES equipment consists of a fixed energy radiation source, a sample, an analyzer, an electron detector, and a high vacuum environment. The radiation source varies depending on the type of PES used. Other devices may be used to enhance analysis, such

as an electron gun and a voltage generator to bias the sample and improve electron collection. Figure 12 shows an example schematic of a PES system.

The photon source is typically an X-ray gun for XPS or an ultraviolet (UV) gas discharge lamp for UPS. The x-rays produced by the x-ray gun in this study came from Mg ($h\upsilon$ = 1235.6 eV). The UV source produced He I ($h\upsilon$ = 21.22 eV) photons.

The analyzer acts as a band pass filter, allowing only electrons of a certain energy range through. This is done via tunable magnetic or electrics fields. Those outside the set range will be deflected and absorbed by the analyzer walls.

The analyzer used in these experiments was a spherical deflection analyzer (SDA). It consists of two concentric hemispheres, as shown in Figure 12. The analyzer is arranged to be able to collect the electron released from the sample by the photoelectric effect. The analyzer is preset to allow the desired electrons in. Before reaching the analyzer, the electrons must first pass through a physical aperture. This is settable to different sizes. The smaller the aperture size, the lower the intensity of the electrons that reaches the analyzer. While the resolution is higher, the aperture is typically set to a low setting for UPS, due to the high intensity of UV produced by the discharge lamp, which in turn generates a large number of ionized electrons. A too high intensity of electrons can damage the analyzer. XPS can be safely used with higher aperture settings.

The electrons must pass another barrier before final entry into the analyzer: the retardation stage. This retardation is essentially a high pass filter, removing low energy electrons which tend to increase noise. The retardation energy for the electrons is constantly adjusted to allow electrons of different energies through and produce a full spectrum of energy levels.

Now the electrons enter the hemispherical analyzer, where they are transported and filtered via the application of an electric field between the two plates. This voltage is kept at a user-defined constant to determine the variance of electron energies that are permitted through, and hence adjusts the resolution of the scan.

An electron detector on the other side of the analyzer then measures the intensity of the electrons at each energy level. The electron detector used in this study is an electron multiplier tube, although micro-channel detectors are also common in PES systems. The electron detector creates a cascade of electrons produced by the initial electrons exiting the analyzer. This is accomplished by a voltage applied in the detector, giving the initial electrons additional energy. These electrons strike the detector wall, creating several more electrons for each initial electron. The process repeats until a cascade of electrons has been created, which reach the end of the detector and are measured.

It should be noted that the work function of the sample is not needed to determine the binding energy of the emitted electrons. Due to a common ground connection, the Fermi levels of the sample and spectrometer are equilibrated, their equilibration confirmed via calibration. Thus, the measured electrons have a binding energy given by:

$$KE = h\upsilon - BE - \Phi_s.$$

where Φ_s is the work function of the spectrometer.

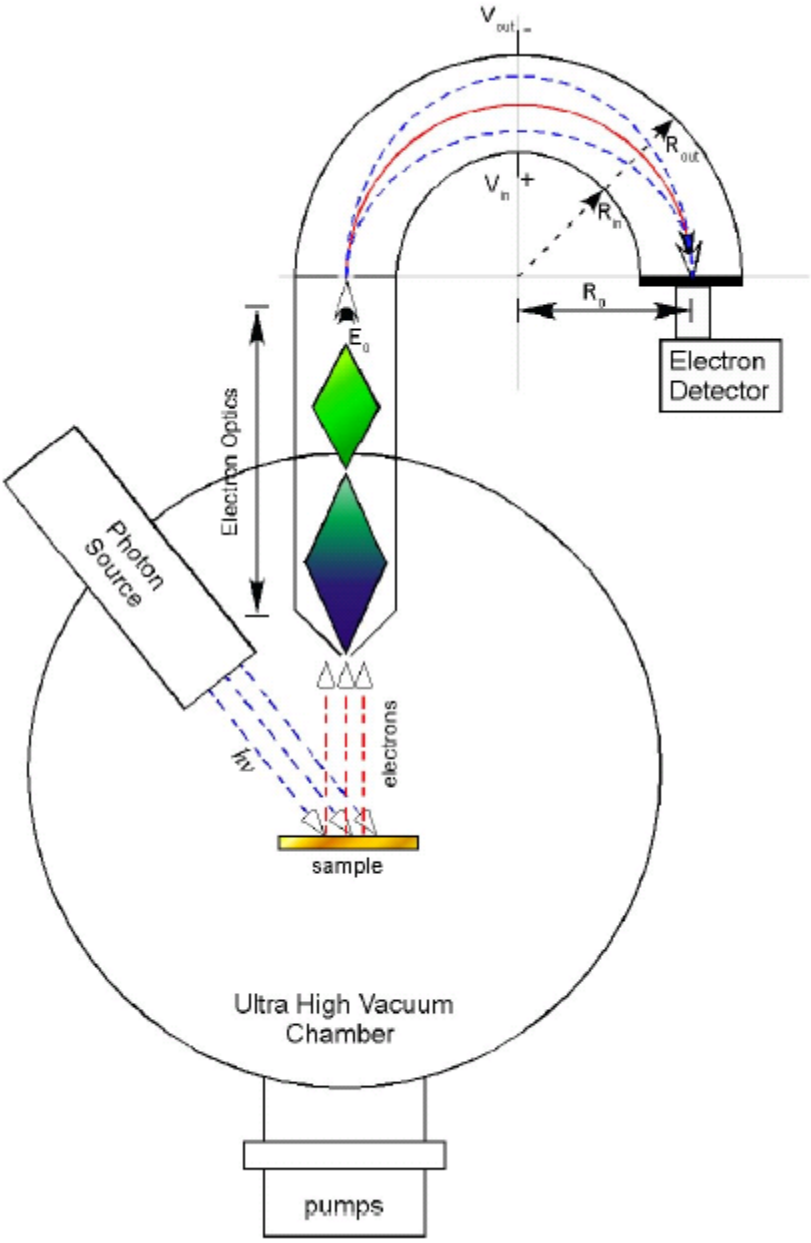

Figure 12: Photoemission Spectroscopy Equipment Schematic (from Reference [33])

The sample is grounded via contact with a sample holder to prevent charging. Lack of grounding of the sample will prevent replacement of the electrons emitted during the emission process, and will leave the sample positively charged, thus ostensibly increasing the binding energy of the electrons as exposure time increases. This ground is

also used as a reference level for the Fermi equilibration of the sample and spectrometer, as described above.

The spectroscopy process is performed in a high vacuum environment to sustain the integrity of a sample's surface composition during measurements. A high vacuum environment will allow the sample to remain contamination-free for up to several days if the pressure is low enough. By contrast, even a few seconds spent in ambient conditions will cause the sample to accumulate contaminants on its surface that will significantly affect the measurements.

X-ray Photoelectron Spectroscopy

X-rays are ideal for probing the core levels of the molecules in a sample due to their high energies. Each element contains electrons at characteristic binding energies that can be measured. Evaluation of the full range of electron energies emitted by the x-rays allows a detailed spectrum of these characteristic energies, and allows a determination of which elements are present in the sample, depending on the orbital peaks present. Given similar ionization cross sections, a higher peak implies a greater number of the element within the sample. Only electrons with binding energies smaller than the x-rays' energy value can be probed, as those with higher binding energies will not receive enough energy to leave the sample.

Figure 13 shows an example of a cleanly sputtered Au sample characterized by XPS. The resulting peaks are all characteristic of Au.

Electrons within the same orbital may produce different binding energies, depending on the configuration of the electrons. These configurations are not equally

probable, and so the result is a cluster of peaks within the same general area which are not symmetric to each other and have differing intensity. The split configuration is always the same for each orbital in an element. One of gold's spin doublets can be seen in Figure 13 between 300 and 400 eV.

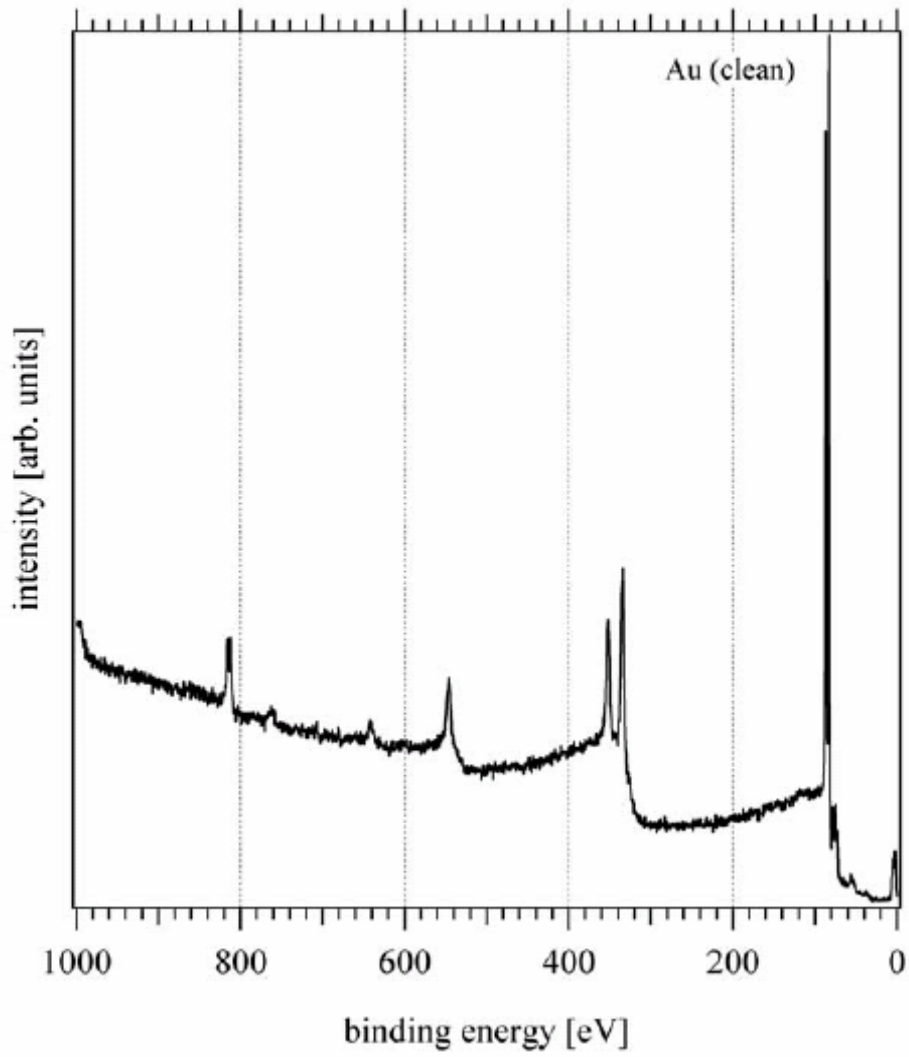

Figure 13: XPS Example, Spectrum of a Clean Gold Sample (from Reference [33])

Changes to a sample's molecular properties can be determined by noting the alterations occurring to the sample's peaks, including shifts to lower or higher binding energies and changes in peak intensity. Figure 14 shows an example of a O1s peak shift and lowering of intensity.

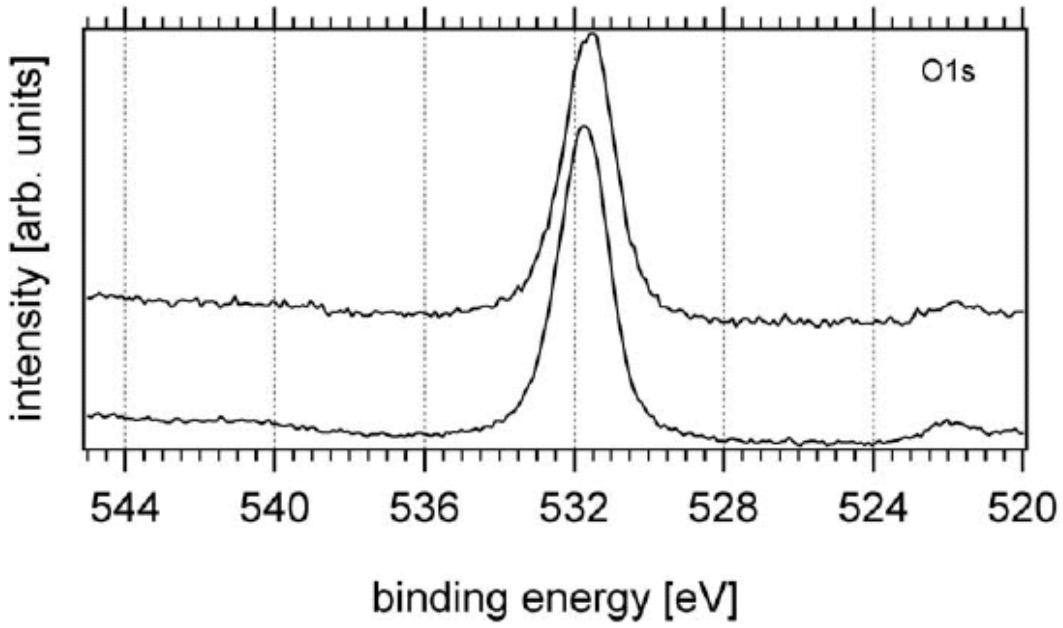

Figure 14: Peak Shift Example, Lowering of O1s Binding Energy After Exposure to X-ray Radiation (from Reference [33])

A secondary technique utilizing XPS is low intensity XPS (LIXPS). LIXPS is a measurement procedure utilizing a greatly reduced photon flux from standard XPS (1.2% of standard XPS photon flux) [34]. LIXPS is used to measure the secondary edges of samples. Since the high intensity of UPS may lead to charging of the sample while measuring secondary edges, LIXPS is performed before and after each UPS measurement to determine whether charging occurred during UPS operation. LIXPS may also be used

in lieu of standard UPS on light-sensitive samples, such as ITO. A bias voltage is typically applied to separate analyzer and sample secondary edges and to collect emitted electrons more efficiently.

Ultraviolet Photoemission Spectroscopy

Ultraviolet photoemission spectroscopy is used to analyze the valence bands of a sample and determine its work function through analysis of the secondary edge. The gas discharge lamp typically used for UPS provides a narrow line width of radiation to the gas's discrete energy structure, and also allows a large photon flux, permitting the process a high resolution and a high ration of signal to noise. He I α is the typical photon used, with an energy of 21.22 eV. UPS is generally used to investigate such properties as the highest occupied molecular orbital (HOMO) and charge injection barriers of a sample. Because of the source of the photons from UPS is a gas, the atoms emit photons in a narrow band of energies, increasing resolution of the resulting spectra and narrowing the peak widths. A bias voltage is typically used in conjunction with UPS to increase the magnitude of the secondary edge and to separate analyzer and sample secondary edges.

Figure 15 shows the UPS spectra of the P3HT/Au interface. The bottom spectra of each of the panels show bare Au, with each successive layer representing a deposition step of P3HT. The center panel displays the complete UPS spectra. The left panel shows the normalized secondary edge of the sample. The large shift after the first deposition is most likely related to the formation of an interface dipole, while the later, more gradual shifts can be attributed to either band bending or charging of the sample. The rightmost panel shows the valence bands of the sample. For the bare Au, large peaks can be seen

which represent the d-bands of the gold. As more P3HT is deposited, these peaks attenuate and P3HT-related characteristic emission arise.

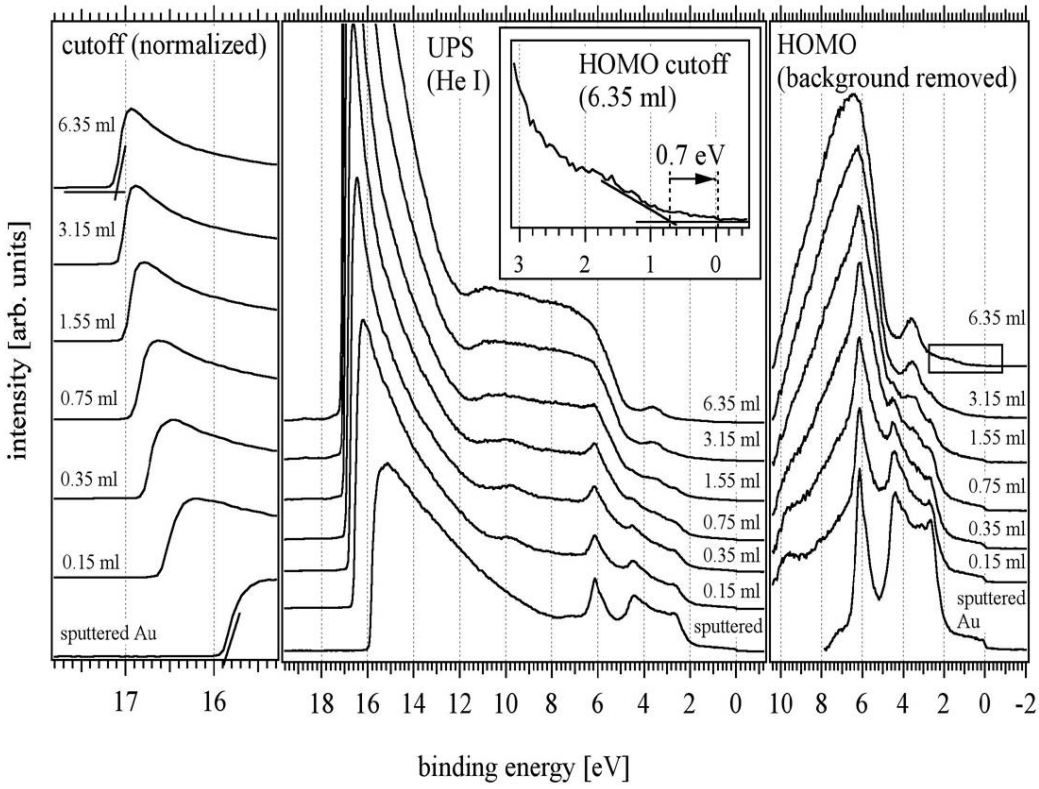

Figure 15: UPS Spectra of the P3HT/Au Interface

Experimental

Three main experiments were performed to investigate the electronic properties of various P3HT interfaces. P3HT was deposited on three substrates: Au, HOPG, and ITO. The ITO experiment was performed differently from the others due to special consideration of the ITO substrate. These experiments will be discussed at length in the following sections, with the ITO experiment explained in detail following the first two.

Experimental Method

All experiments were performed in an ultra high vacuum (UHV) system, shown in Figure X. The system was composed of four chambers: a fast entry lock, a preparation chamber, a deposition chamber, and an analysis chamber. The system was acquired from SPECS (Berlin, Germany). The base pressures of the chambers were $1x10^{-10}$ for the analysis chamber, $1x10^{-8}$ for the preparation chamber, and $1x10^{-7}$ for the entry and deposition chambers. The system was pumped with turbomolecular/rotary pumps in combination with ion pumps. The preparation chamber contained a SPECS IQE 11/35 ion source for Ar^{+} ion sputtering. The analysis chamber was equipped with a SPECS non-monochromated XR 50 dual x-ray gun for XPS, a SPECS UVS 10/35 ultraviolet source for UPS, and a SPECS Phoibos 100 hemispherical analyzer. Igor Pro software (Wavemetrics, Inc.) was used for all evaluation, graphing, and curve fitting.

The P3HT was prepared in a toluene solution at 0.1 mg/ml and kept wrapped in an aluminum cover to avoid exposure to light. The P3HT had a weight-average

molecular weight (M_w) of 19 398 with a polydispersity index (M_w/M_n) of 1.59 as determined by gel permeation chromatography (GPC) based on polystyrene standards. 100nm thick Au films were created via thermal evaporation on Si wafers. The ITO and HOPG substrates were purchased from Mikromasch USA ("ZYA" quality), and X, respectively. A 5 V bias was applied to the samples during UPS and LIXPS to separate the analyzer and sample secondary edges. Mg Kα (hυ = 1235.6 eV) radiation was used for the XPS measurements, and He I (hυ = 21.22 eV) for the UPS measurements. The PES measurements were analyzed via a SPECS Phoibos 100 hemispherical analyzer. Peaks were fit using a Gauss-Lorentzian profile, as outlined by Kojima and Kurahashi [35]. Work function and HOMO cutoffs were determined by fitting a line tangent to the curve of the cutoff and evaluating its intersection with the energy axis of the spectra. Analyzer broadening was corrected by adding 0.1 eV to the fitted cutoff values.

Sample Preparation

For each experiment, the substrates were sonicated in acetone, iso-propanol, and methanol, and then dried. The substrates were then mounted onto a sample holder using conductive silver epoxy. For the Au and ITO samples, a small spot of silver epoxy provided an electrical contact between the sample and the holder to allow a path to ground. Once inside the UHV system, the HOPG sample was cleaved to provide a contamination-free surface.

Au and HOPG Analysis Procedure

Each sample was placed into the fast entry load lock. After stabilization of pressure, the sample was moved to the preparation chamber, where it was sputtered with Ar^+ ions for 30-60 minutes. The sample was then transferred to the analysis chamber. LIXPS was performed on the sample, followed by UPS and then another LIXPS investigation. The LIXPS experiments were performed to ensure no charging occurred during the high intensity UPS investigation. Following this, XPS was performed, first as a survey scan on the entire energy range available to XPS, and then as intense, focused investigations on orbital peaks of particular importance to the analysis of the sample and the eventual P3HT deposition.

After this initial analysis, the sample was transferred to the deposition chamber, where it was prepped for deposition of P3HT. A laser crosshair was utilized for correct positioning of the sample.

A syringe filled with P3HT solution was placed onto a syringe pump, where it was injected into the electrospray chamber through a capillary. The injection rates were 10 ml/h for the Au and HOPG samples and 4 ml/h for the ITO sample. The electrospray capillary was biased at -3.5 kV relative to the grounded chamber. N_2 gas was pumped into the electrospray enclosure around the orifice to prevent exposure to ambient contamination.

After initial deposition, the sample was transferred back to the analysis chamber, where the previous PES steps were again performed. This procedure was performed several times, with seven depositions of P3HT solution on the Au substrate (for a total of 6.35 ml) and five depositions on the HOPG substrate (for a total of 3.15 ml).

ITO Analysis Procedure

It has been observed that high intensity UV and x-rays significantly reduce the work function of ITO substrates [34, 36]. Due to this limitation, only LIXPS was performed on the ITO substrate during P3HT deposition. The substrate also was not sputter cleaned, as this procedure also affects changes in the work function. Upon first loading and after each deposition, LIXPS was performed on the sample. These were done as quickly as possible to prevent unnecessary exposure to x-rays. A total of seven depositions were performed, resulting in a total of 6.45 ml of P3HT solution injected into the electrospray chamber. After the final LIXPS measurement, UPS was performed to examine the effects of high intensity UV light on the ITO work function.

To measure the effects of x-ray exposure on ITO, two more ITO substrates were examined. The first was exposed to LIXPS 24 times, the measurements being performed as the exposure took place. The second was exposed to high intensity x-rays. Each exposure time was double the previous one, with the first exposure time set to 30 seconds. A total of six exposures were performed, with LIXPS performed between each exposure to evaluate the secondary edge shifts that occurred during exposures.

Results and Discussion

P3HT/HOPG Results

Figure 15 shows the S2p core level spectra of the P3HT/HOPG thin film. From first to last P3HT deposition, the S2p doublet shifts from a starting position of 163.88 eV to 164.0 eV, a total of 0.12 eV, most likely related to band bending at the interface. The magnitude of the peak also increases as P3HT is deposited, from the sulfur atom present inside the chain of a thiophene monomer.

Figure 16 displays the UPS spectra of the P3HT/HOPG junction. The center panel displays the complete UPS spectra. The rightmost panel shows a normalized close up of the secondary cutoff. The secondary edge shifts from 16.60 eV (vacuum-cleaved HOPG) to 16.77 eV, indicating a reduction in the work function 0.17 eV, most likely related to band bending and a small interface dipole (small due to the stable nature of HOPG). The rightmost UPS panel shows the valence band spectra of the interface, with background removed. A transition from HOPG to P3HT-dominant emissions reveals a weak P3HT HOMO shoulder of 0.41 eV.

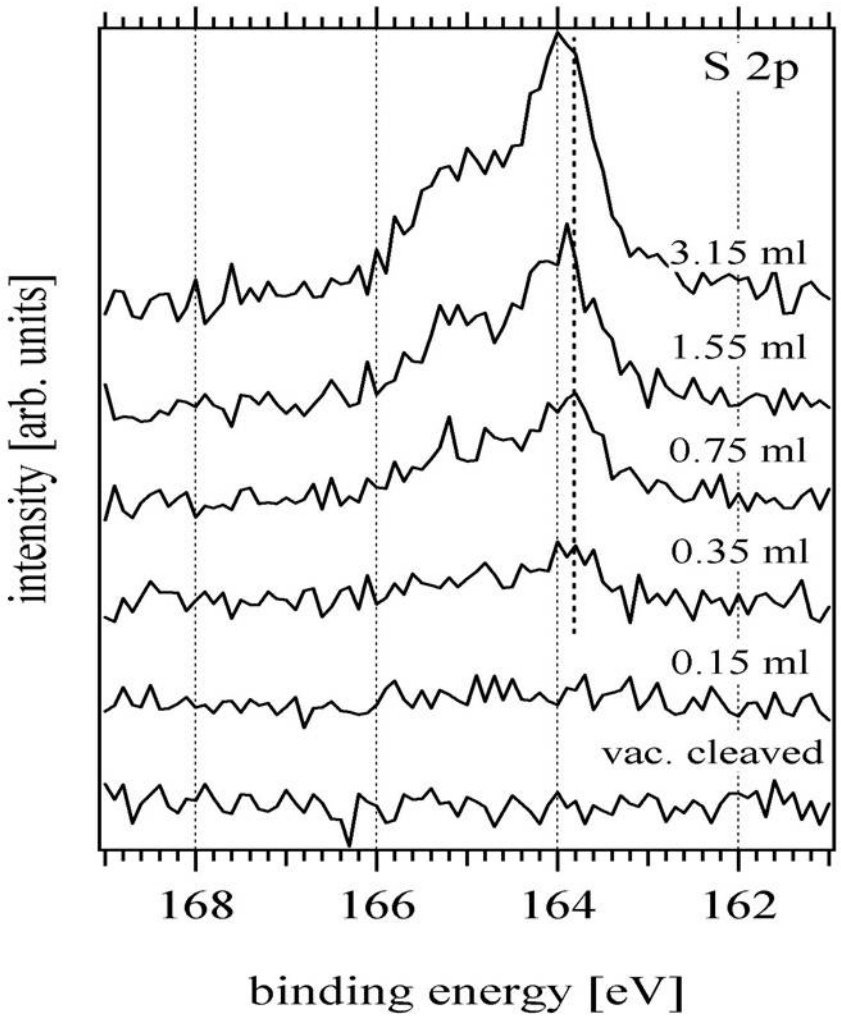

Figure 16: S2p XPS Core Level Spectra for P3HT/HOPG Interface

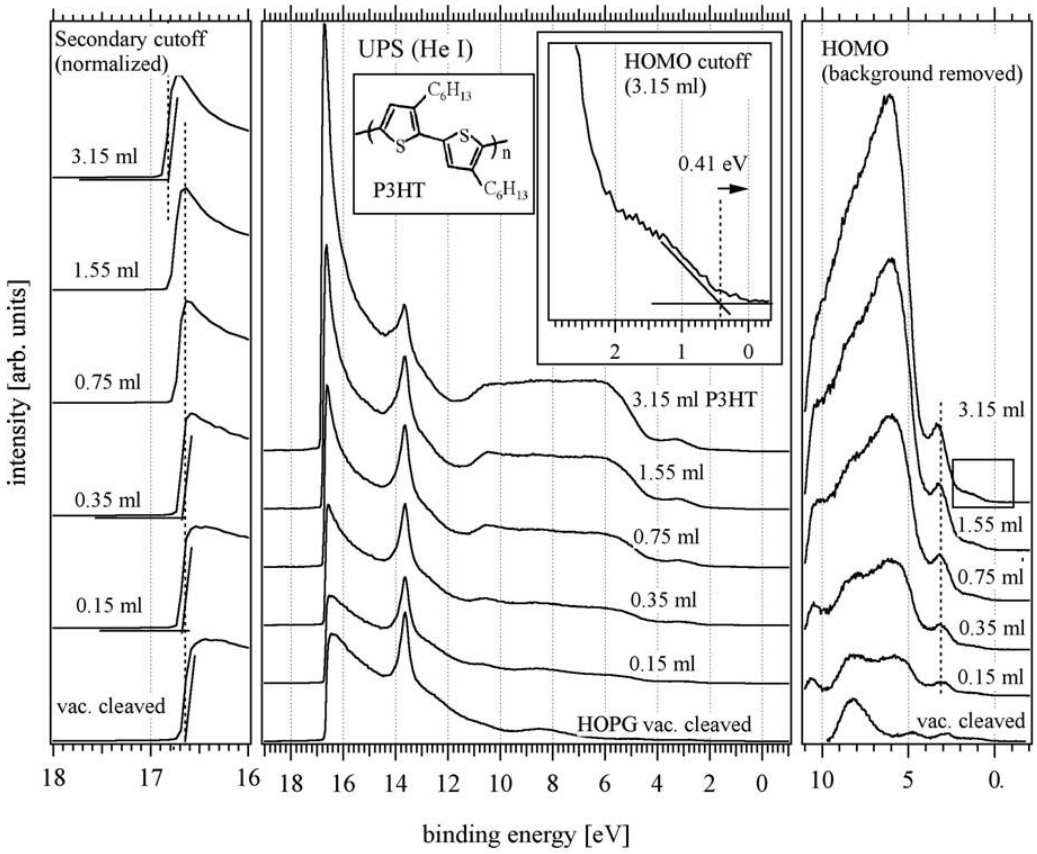

Figure 17: UPS Spectra for P3HT/HOPG Interface

P3HT/HOPG Discussion

The UPS and XPS data of the P3HT/HOPG interface can be analyzed to construct an orbital lineup diagram of the junction. The UPS data in Figure 16 show the shift in the secondary edge as P3HT is deposited. A very gradual shift throughout the deposition process implies a lack of strong charging and a small or negligible interface dipole. Since the weak emission of the S 2p peak makes it an unreliable benchmark for band bending, the secondary edge shift is used to determine the amount of band bending, showing a shift of 0.17 eV from first to last deposition. This shift includes both band bending and

interface dipole, however. The dipole can be estimated by taking the work function of the pristine HOPG (Ψ_{HOPG} = 4.61 eV) and comparing it to the work functions of the first two depositions, which yielded values of 4.57 and 4.53 eV. This implies an interface dipole of between 0.04 and 0.08 eV, which when subtracted from the total work function shift of 0.17 eV yields band bending values of 0.09-0.14 eV. The average of these values (0.12 eV) is in perfect agreement with the shift of the S 2p peak.

The ionization energy of the P3HT was determined by adding the work function of the 3.15 ml layer with the HOMO cutoff position (0.41 eV), yielding a value of

4.44 eV + 0.41 eV = 4.85 eV

This is in reasonable agreement with the ionization energy value found in the P3HT/Au experiment. This value was used for the ionization energy of the P3HT/ITO experiment, because of the difficulty in evaluating the ionization energy in the ITO experiment.

The hole injection barrier at the interface can be determined by subtracting the band bending (0.12 eV) from the HOMO cutoff position (0.41 eV), yielding a value of 0.29 eV. The electron injection barrier Φ_e = 1.41 was determined by subtracting the hole injection barrier from a previously discovered optical band gap of E_g = 1.7 eV, determined by UV-visible spectroscopy [X]. This should be taken as a lower limit for the electron injection barrier, as the optical band gap (by the exciton binding energy) is smaller than the polaron band gap, which should be used for the band gap. The resulting data gathered and analyzed was used to construct an orbital lineup diagram of the interface, Figure 17.

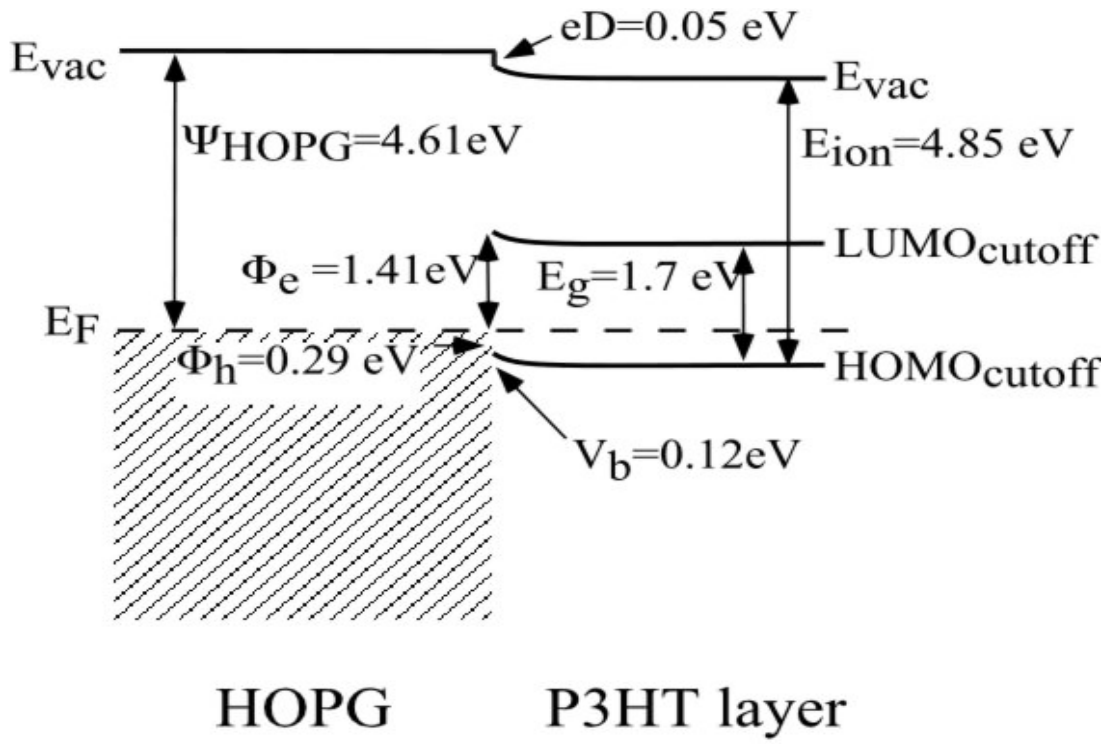

Figure 18: Orbital Lineup of the P3HT/HOPG Interface Constructed from the UPS and XPS Data Set

P3HT/Au Results

Figure 18 shows the XPS spectra of the P3HT/Au interface core levels. The bottom spectra represent the bare, sputtered Au substrate. Each of the following spectra was measured after each P3HT deposition step. The graph shows the C1s, S2p, and Au4f core levels, from left to right. A small carbon peak can be seen in the C1s spectrum before deposition. This is most likely related to contamination of hydrocarbons that failed to be removed during sputtering. After the first deposition, two peaks emerge. One is the initial carbon peak of the nascent P3HT thin film. The other appears to be residual toluene solvent adsorbed onto the substrate during the deposition sequence.

During the last three depositions, the C1s peak shifts to the left 0.11 eV (determined by peak fitting), which may be an indication of band bending. The S2p and Au4f show similar shifts. The Au4f peaks also attenuate during deposition as the gold is covered by the P3HT film.

Figure 19 shows the UPS spectra of the P3HT/Au interface. The central panel shows the spectra in their entirety. To the left, a normalized close up of the interface secondary edge is presented. A strong shift is present after the first deposition, which is most likely related to an electric dipole formed from the compression of the electron cloud around the metal surface. After this initial jump, a slower shift to the right can be seen, more likely due to band bending rather than charging because the shift saturates as more P3HT is deposited. The rightmost panel displays the valence bands spectra. The sharp peaks visible in the valence band are the Au sample's d-orbitals. As the P3HT thin film grows, the Au valence band features attenuate and P3HT HOMO features arise. The HOMO cutoff of the final P3HT thin film is measured to be 0.7 eV.

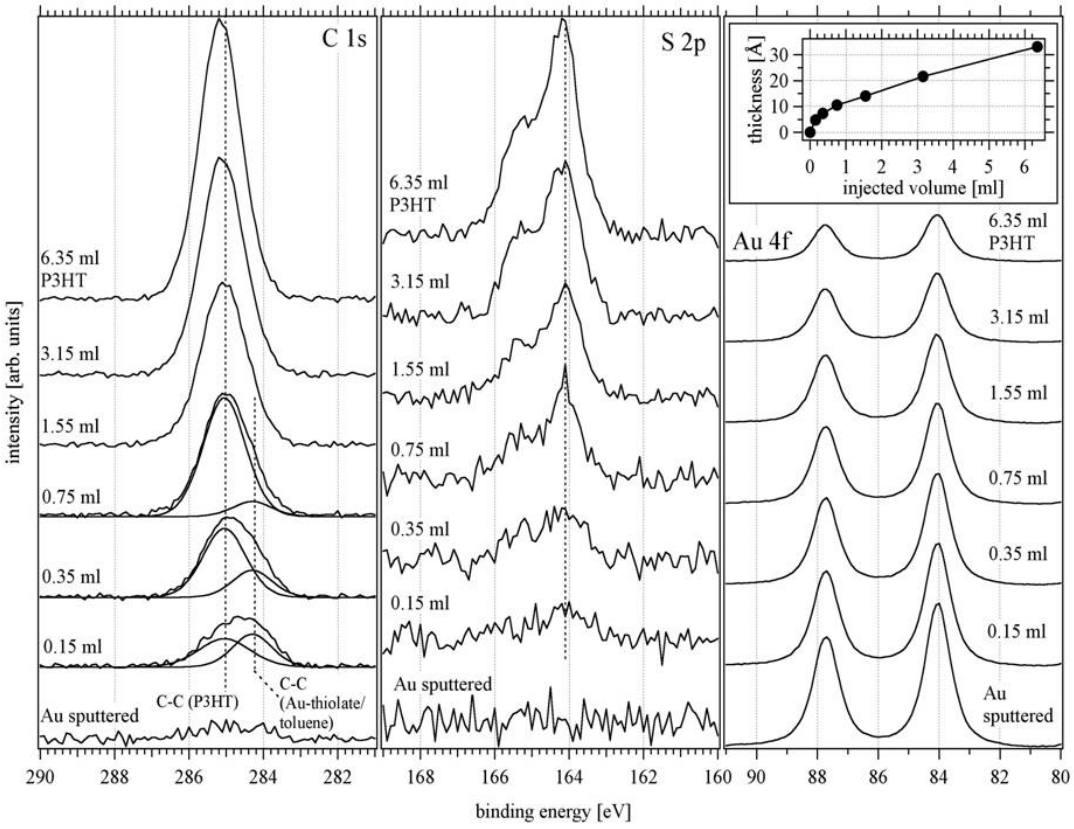

Figure 19: XPS Core Level Spectra for P3HT/Au Interface

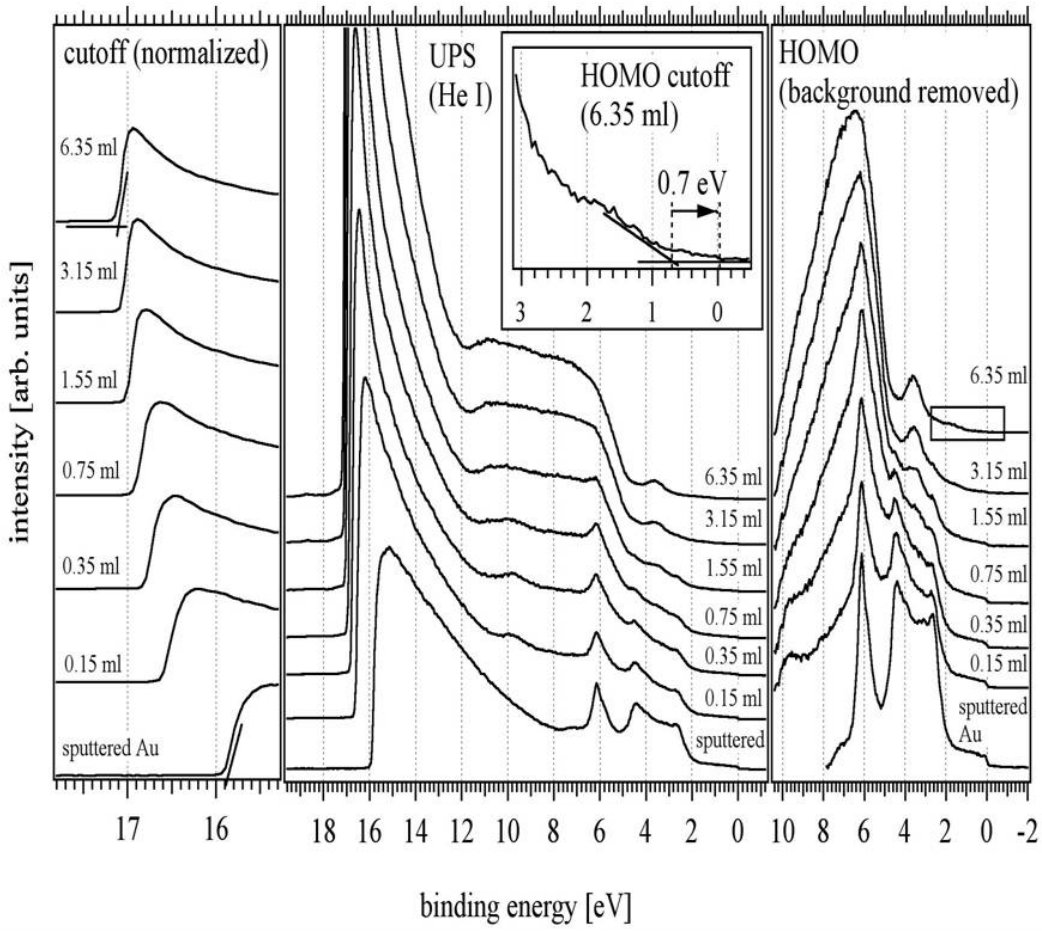

Figure 20: UPS Spectra for P3HT/Au Interface

P3HT/Au Discussion

Evaluation of the P3HT/Au photoemission spectroscopy measurements gives us a detailed look at the electronic properties of the interface. The UPS spectra, shown in Figure 19, display the work function and the HOMO value of the junction before and after each deposition. The spectrum of the sputtered Au (bottom spectrum) is characteristic of Au UPS emissions, with prominent peaks representing the *d*-bands of the Au. New features arise on top of the gold peaks as the P3HT is deposited. These

features have been related earlier to bonding orbitals of the alkyl ligands (bands >5 eV), sulfur related localized states (peak at ~3.8 eV), and backbone related localized states (shoulder at ~1 eV) [37, 38].

After the first deposition, the secondary edge of the interface experiences a strong shift to the left. This shift is most likely related to an interface dipole, caused by the electron gas surrounding the metal being pushed into the metal surface by the P3HT overlayer and thus reducing the metal work function [39].

The XPS spectra shown in Figure 18 show the C1s, S2p, and Au4f peaks of the interface during P3HT deposition. The bottom C1s spectrum shows a weak signal present before P3HT deposition, probably related to ambient contamination missed by the sputter cleaning. After the first deposition (0.15 ml), a two component peak arises, the lower energy peak corresponding to a small amount of Toluene solvent coadsorbed during deposition. The P3HT C1s peak continues to strengthen after each deposition, and shifts slightly during the last three depositions a total of 0.11 eV. This is due to the occurrence of band bending as the Fermi levels of the polymer layer and substrate equilibrate. A similar shift is seen for the S2p peak. Charging is ruled out because the shifting saturates instead of accelerates, and no similar shift is seen in the UP spectra, where much higher magnitudes of photon intensity are used. No x-ray damage is presumed because none of the XPS peaks show typical shape degradation after severe x-ray exposure [40].

Using the information garnered from the XPS and UPS spectra, an electronic interface diagram can be constructed. Figure X shows a summary of the evaluation. The hole injection barrier Φ_h was determined by subtracting the band bending of the polymer

at the interface V_b from the fitted HOMO cutoff of the 6.35 ml spectrum, giving an injection barrier of

$$\Phi_h = 0.7 \text{ eV} - 0.11 \text{ eV} = 0.59 \text{ eV}$$

This evaluated barrier is considerably larger than previously reported studies of the P3HT/Au interface [41], which determined a barrier of 0.3 eV. This difference may result from different preparation methods or the presence of ambient contamination at the interface [42]. The secondary cutoff of the 6.35 ml spectrum was determined to be at 17.02 eV (corrected for analyzer broadening), yielding an ionization energy E_{ion} of 4.90 eV. This was generated by finding the work function from the secondary edge and adding the HOMO cutoff value to it.

The electron injection barrier was Φ_e determined using a previously calculated optical energy gap of 1.7 eV [43]. Subtracting the hole injection barrier from this value yielded the result

$$\Phi_e = E_g - \Phi_h = 1.7 \text{ eV} - 0.59 \text{ eV} = 1.11 \text{ eV}$$

This is a lower limit for the electron injection barrier since the optical gap is typically smaller than the polaron gap, which is the correct gap to use to account for the exciton binding energy. The interface dipole eD was calculated by subtracting the hole injection barrier from the ionization energy of the polymer and then subtracting this total from the work function of the Au. Thus,

$$eD = \Psi Au - (E_{ion} - \Phi_h) = 5.31 \text{ eV} - (4.89 \text{ eV} - 0.59 \text{ eV}) = 1.01 \text{ eV}$$

This is a sizable interface dipole, and shows a strong chemical reaction between the Au and the P3HT.

Comparison of these data with similar oligomer-based thiophene/Au investigations yields interesting conclusions. A paper by *Fujimoto et al.* analyzes the results of HOMO density of state changes with changes in oligomer chain length [44]. Comparison with their UP data on octithiophene bears a close similarity with our polymer measurements, the primary difference being a more spread out HOMO cutoff on the polythiophene, suggesting a stronger dispersion of the HOMO band due to its longer chain length. Chandekar and Whitten [8] have reported an inverse relationship between the oligothiophene chain length and the hole injection barrier values, i.e. a higher chain length results in a smaller injection barrier. Their data on the sexithiophene oligomer show a hole injection barrier of 1.1 eV, significantly larger than the measured 0.7 eV of the final deposition step in the polymer experiments. They also report an ionization energy of 5.2 eV, a difference of 0.6 eV from our reported ionization energy. This suggests a symmetrical increase in their hole and electron barriers from ours.

Another study done by Schwieger *et al.* [45] reports a more significant difference between the the oligomer and polymer interfaces structures, reporting a 1.2 eV work function shift during deposition of a sexithiophene overlayer, suggesting a larger interface dipole. Their data shows a hole injection barrier of 1 eV, a measurement similar to the one in reference 8.

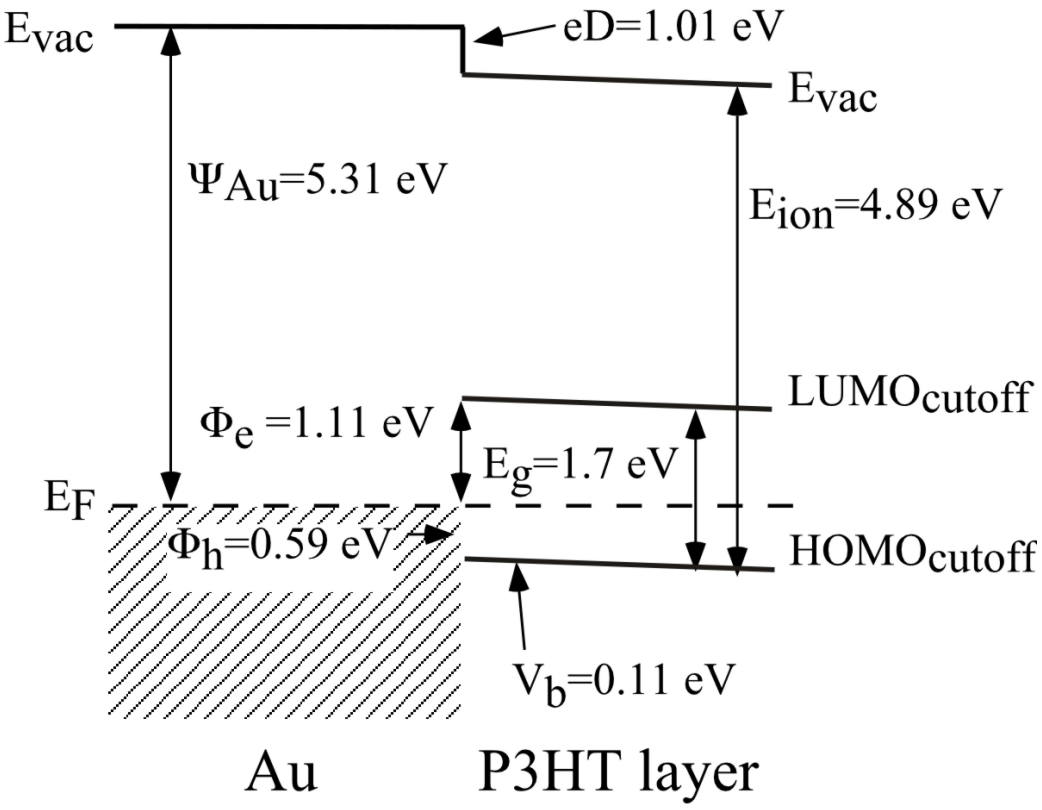

Figure 21: Orbital Lineup of the P3HT/Au Interface Constructed from the UPS and XPS Data Set

P3HT/ITO Results

Figure 21 shows the results of the ITO work function shifts when exposed to LIXPS. A total of 24 measurements were performed, in succession and as quickly as possible to keep the time between measurements consistent. The work function of the ITO was reduced by 0.18 eV during the course of the experiment.

Figure 22 displays the ITO work function shifts when exposed to standard intensity x-rays, as measured by LIXPS. Seven measurements were performed, each one after a period of x-ray exposure double the previous time, beginning with a 30 second exposure. The leftmost panel shows the shift of the secondary edge caused by the x-ray exposure, while the right panel shows a graph of x-ray exposure time versus work

function of the ITO sample. A total shift of 0.53 eV was observed over the course of the exposures.

Figure 23 shows the results of LIXPS measurements performed on an ITO sample upon which P3HT was deposited. A total of seven depositions were performed, between which LIXPS measurements were carried out. After the final LIXPS measurement, a UPS measurement was performed. The leftmost panel shows the secondary shift of the sample as the P3HT was deposited. A total shift of 0.17 eV was detected between the first and last LIXPS measurement. The UPS measurement reduced the work function an additional 0.59 eV. The middle panel shows the UPS spectra measured after the final LIXPS measurement. The rightmost panel shows the HOMO region of the ITO sample after the final UPS exposure, pinning the HOMO cutoff at 0.81 eV (middle panel inset).

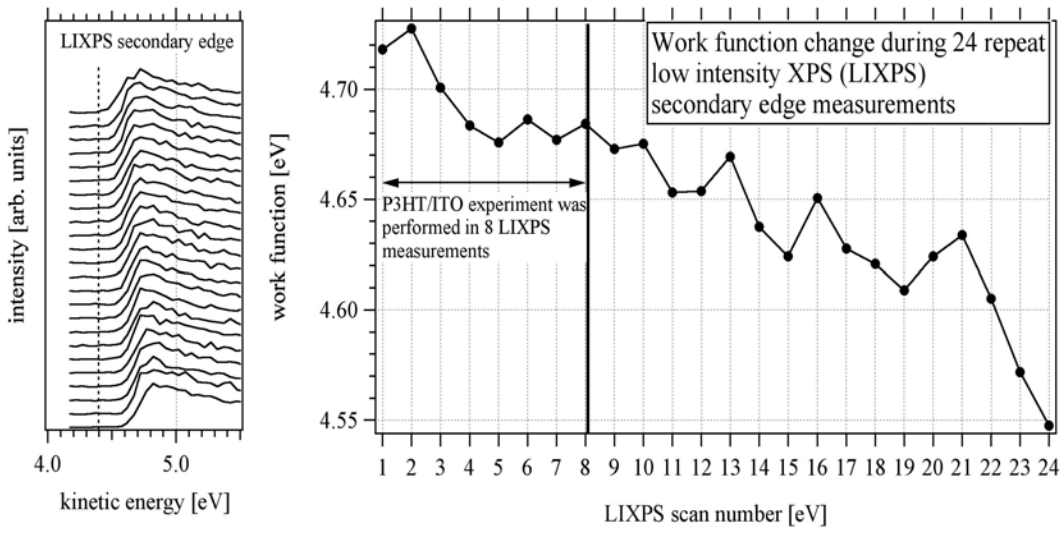

Figure 22: ITO Work Function After Light Intensity X-ray Exposure

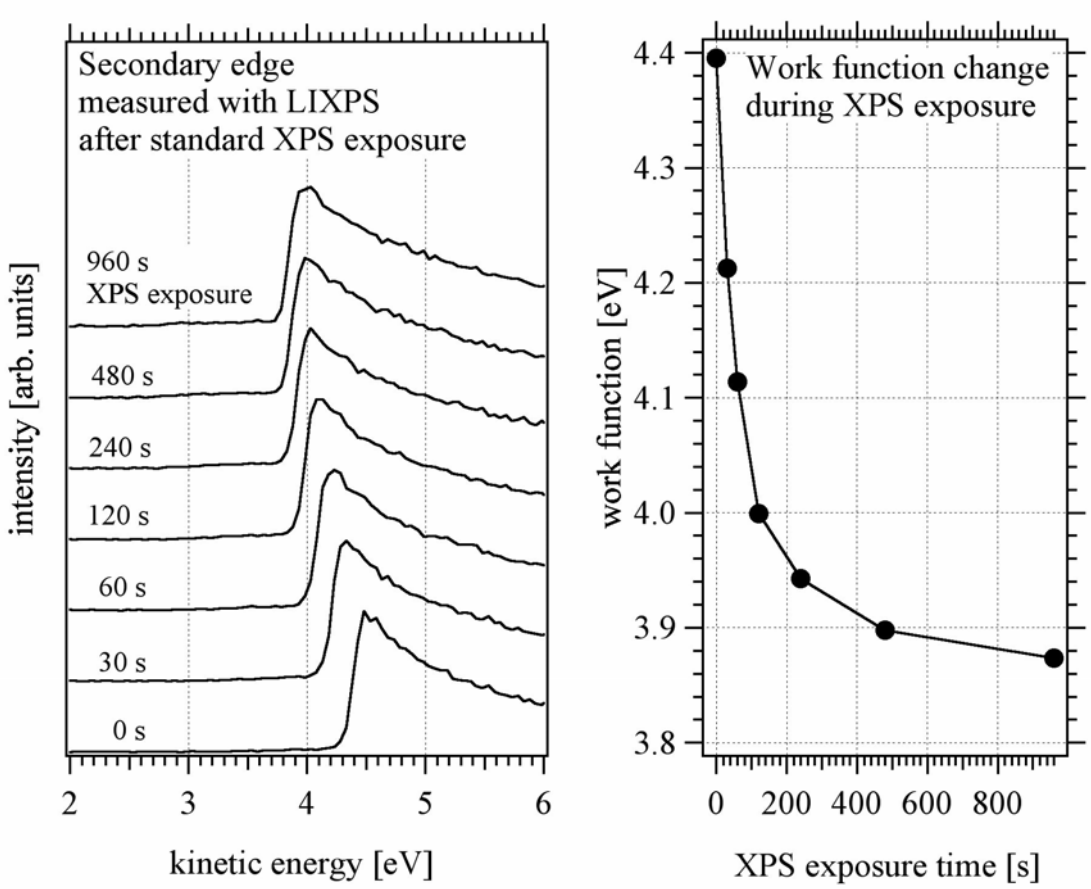

Figure 23: LIXPS Measurements of ITO Sample After Exposure to Standard Intensity X-rays

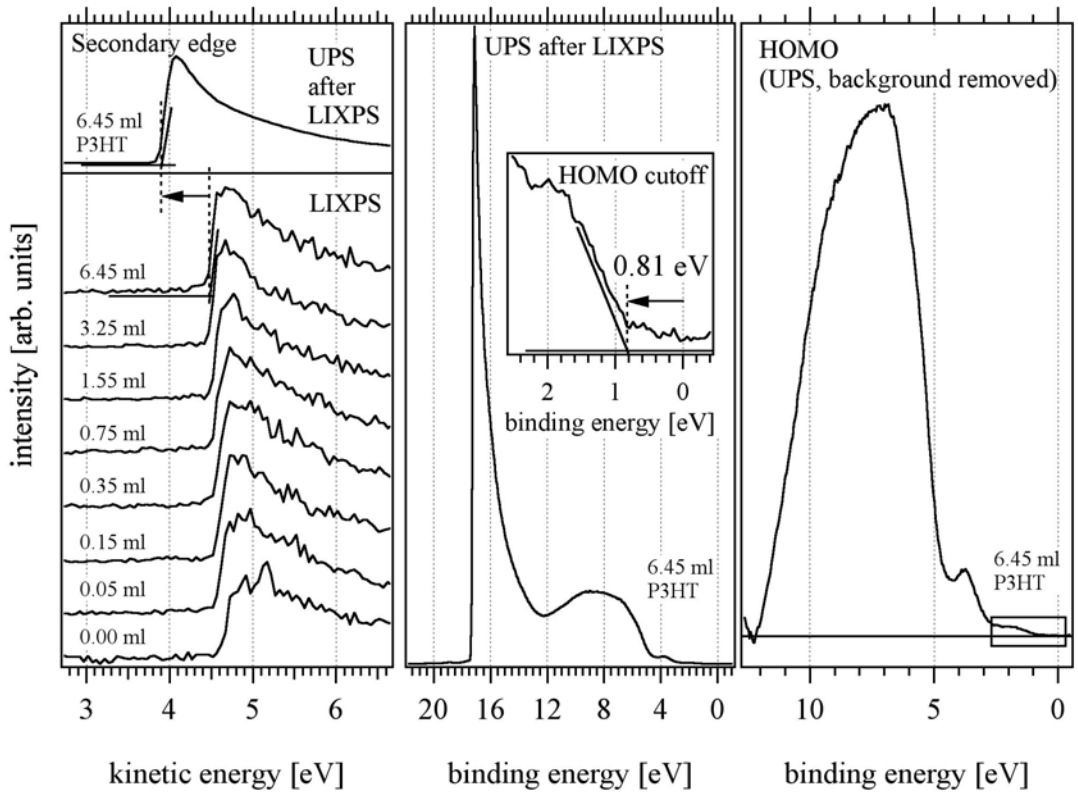

Figure 24: LIXPS and UPS Spectra for P3HT/ITO Interface

P3HT/ITO Discussion

Given the data on ITO work function alteration from repeated x-ray exposure, it was determined that LIXPS measurements would not change the work function significantly. Over the course of 18 consecutive LIXPS measurements, the work function of the ITO decreased 0.18 eV. Since only eight LIXPS measurements were planned for the P3HT/ITO experiment, the work function change during the first eight LIXPS measurements was also recorded. As seen in Figure 21, the alteration in work function during the first 10 scans is much less than in the subsequent 14, suggesting that reliable measurements could be obtained if the number of LIXPS scans was kept below 10.

A similar experiment to determine the reliability of standard XPS measurements found a shift of 0.53 eV after only six steps, an unacceptable deviation, and so standard XPS was ruled out for the measurement of the P3HT/ITO interface. A substantial deviation in ITO work function caused by a single UPS measurement also ruled out the use of UPS as a mechanism to further examine the interface, leaving LIXPS as the only viable option.

Given the data available gathered from LIXPS measurements of the emerging P3HT overlayer, the orbital band lineup of the interface could be constructed. The valence band minimum (VBM) and conduction minimum (CBM) needed to be determined first. We calculated the VBM relative to the Fermi level by using the In $3d_{5/2}$ peak located at 445.04 eV, since the VBM could not be determined by valence band spectra due to superimposed P3HT emissions. The known energy difference between the X peak and the VBM [15] is 441.8 eV, giving a VBM of 3.24 eV, which is in agreement with recent results [46]. Using an optical gap of 3.6 eV [15], the CBM was determined to be 0.36 eV.

We used the previously measured ionization energy from the HOPG experiment of 4.85 eV for constructing the P3HT/ITO lineup, because of the difficulty in analyzing the ionization energy from the ITO data. Using this and other data, the interfacial orbital lineup was constructed, shown in Figure 24. The work function of the sample decreases 0.17 eV from the bare ITO to the last P3HT deposition. This shift probably contains a LIXPS induced work function reduction of 0.05 eV corresponding to 8 LIXPS scans (Figure 21). This gives a total of 0.12 eV work function reduction, which is most likely due to a weak interface dipole eD. Using the P3HT ionization energy and aligning the

ITO and P3HT vacuum levels (taking the dipole into account), we determined the HOMO cutoff of the P3HT layer to be 0.25 eV below the Fermi level. Subtracting the HOMO cutoff position from the ITO VBM (3.24 eV), a VBM to HOMO offset of 2.99 eV was determined. The lowest occupied molecular orbital (LUMO) of the P3HT was calculated to be 1.45 eV above the Fermi level by using the P3HT optical gap of E_g = 1.7 eV as determined by UV-vis absorption [43]. The ITO CBM to P3HT LUMO distance was calculated to be Φ_e = 1.09 eV, a lower estimate since optical band gap measurements include excitonic features, resulting in generally smaller band gaps than those actually encountered by charge carriers.

The UPS measurement performed after the final LIXPS measurement further altered the configuration of the interface, as seen in Figure 24. UV exposure reduced the ITO work function 0.59 eV, for a total reduction of 3.96 eV. This implies a new interface dipole eD = 0.76 eV. Band bending is ruled out as an explanation, as earlier investigations [34] showed no shifts in core levels during XPS core level measurements. The new HOMO level after UPS measuring was determined to be 0.81 eV (Figure 24, insert). This implied a new ionization energy of 4.77 eV for the P3HT layer, a small change from the earlier 4.85 eV [47]. This deviation possibly results from weak charging artifacts, since small work function areas dominate secondary edge measurements, while primary peaks represent a true average over all areas of a sample. Figure 24 Shows the new orbital band lineup diagram after UV exposure. The larger interface dipole shifted the features of the interface down to approximately 0.6 eV lower binding energies.

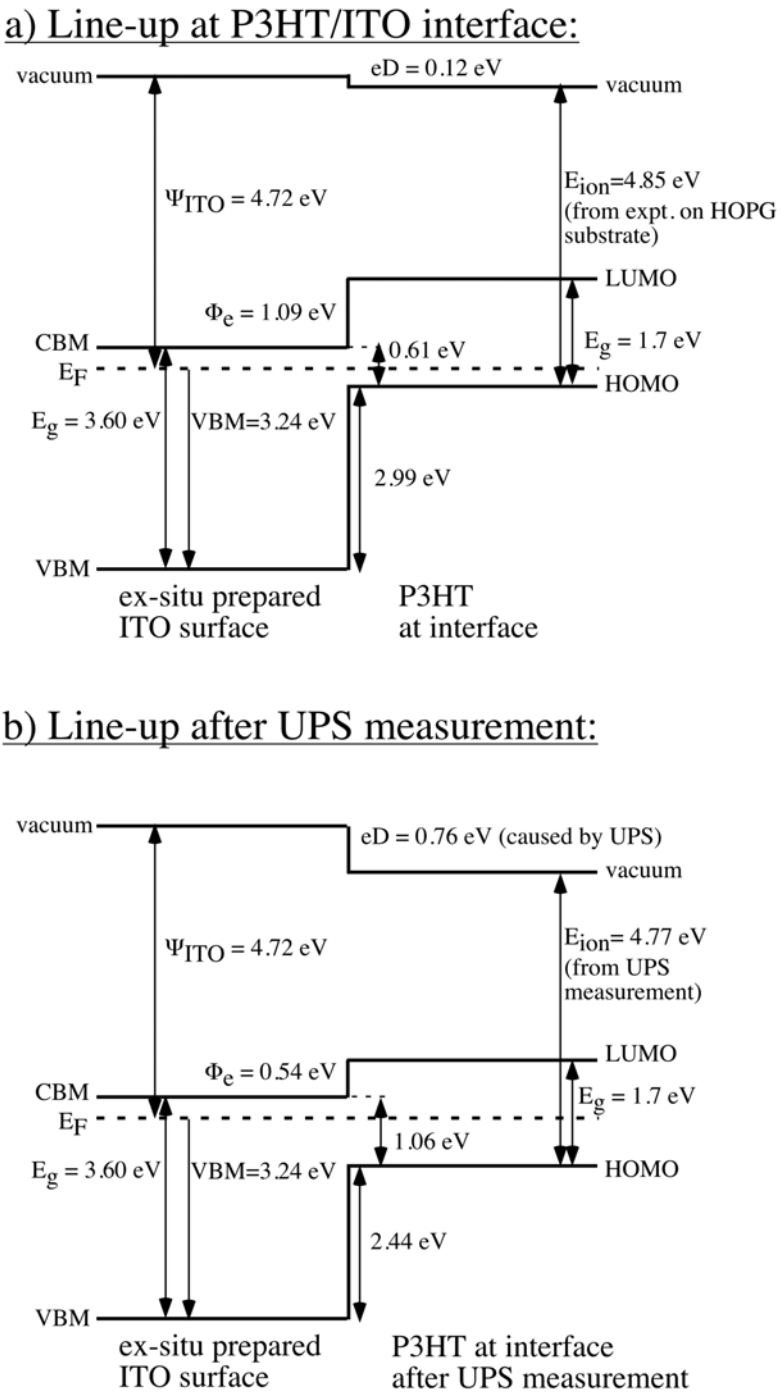

Figure 25: Orbital Lineup of the P3HT/ITO Interface Before and After UPS Exposure

Conclusion

P3HT/Au

In this experiment P3HT was deposited onto a clean Au surface in several steps, with x-ray and ultraviolet photoemission spectroscopy performed between each step. The measurements were performed in situ in an ultra high vacuum environment. Once a suitable layer of P3HT was grown, the data were analyzed using Igor Pro software and an orbital band lineup diagram was created. Several of the properties of the interface were measured, including the HOMO, charge injection barriers, and the presence of absence of interface dipoles. The P3HT interface was found to have slightly modified electronic properties from similar oligomeric interfaces.

P3HT/HOPG

In this experiment P3HT was deposited onto a cleaved HOPG surface in several steps, with x-ray and ultraviolet photoemission spectroscopy performed between each step. The measurements were performed in situ in an ultra high vacuum environment. Once a suitable layer of P3HT was grown, the data were analyzed using Igor Pro software and an orbital band lineup diagram was created. Several of the properties of the interface were measured, including the HOMO, charge injection barriers, and the presence of absence of interface dipoles.

P3HT/ITO

In this experiment bare ITO was exposed to light and standard intensity x-rays to determine their effect on the ITO's work function. P3HT was deposited onto a second ITO substrate in several steps, with light intensity x-ray spectroscopy performed between each step. The measurements were performed in situ in an ultra high vacuum environment. Once a suitable layer of P3HT was grown, the data were analyzed using Igor Pro software and an orbital band lineup diagram was created. Several of the properties of the interface were measured, including the HOMO, charge injection barriers, and the presence of absence of interface dipoles.

References

1. Huynh, W.U., J.J. Dittmer, and A.P. Alivisatos, *Hybrid Nanorod-Polymer Solar Cells*. 2002. p. 2425-2427.

2. Hoppe, H. and N.S. Sariciftci, *Organic solar cells: An overview.* Journal of Materials Research, 2004. 19(7): p. 1924-1945.

3. Stutzmann, N., R.H. Friend, and H. Sirringhaus, *Self-Aligned, Vertical-Channel, Polymer Field-Effect Transistors*. 2003. p. 1881-1884.

4. Tanase, C., et al., *Unification of the Hole Transport in Polymeric Field-Effect Transistors and Light-Emitting Diodes.* Physical Review Letters, 2003. 91(21): p. 216601.

5. Waldrop, J.R. and R.W. Grant, *Semiconductor Heterojunction Interfaces: Nontransitivity of Energy-band Discontiuities.* Physical Review Letters, 1979. 43(22): p. 1686.

6. Salaneck, W.R., et al., *The electronic structure of polymer-metal interfaces studied by ultraviolet photoelectron spectroscopy.* Materials Science & Engineering R-Reports, 2001. 34(3): p. 121-146.

7. Atreya, M., et al., *In situ x-ray photoelectron spectroscopy studies of interactions of evaporated metals with Poly(p-phenylene vinylene) and its ring-substituted derivatives*. 1999, AVS. p. 853-861.

8. Chandekar, A. and J.E. Whitten, *Ultraviolet photoemission and electron loss spectroscopy of oligothiophene films.* Synthetic Metals, 2005. 150(3): p. 259-264.

9. Fujimoto, H., et al., *Ultraviolet photoemission study of oligothiophenes: pi-band evolution and geometries*. 1990, AIP. p. 4077-4092.

10. Cascio, A.J., et al., *Investigation of a polythiophene interface using photoemission spectroscopy in combination with electrospray thin-film deposition*. 2006, AIP. p. 062104.

11. Lyon, J.E., et al., *Photoemission study of the poly(3-hexylthiophene)/Au interface*. 2006, AIP. p. 222109.

12. Yi, Y., et al., *Characterization of indium tin oxide surfaces and interfaces using low intensity x-ray photoemission spectroscopy*. 2006, AIP. p. 093719.

13. Kasap, S.O., *Principles of Electronic Materials and Devices*. 2002.

14. Ishii, H., et al., *Energy level alignment and interfacial electronic structures at organic/metal and organic/organic interfaces (vol 11, pg 605, 1999).* Advanced Materials, 1999. 11(12): p. 972-972.

15. Gassenbauer, Y. and A. Klein, *Electronic surface properties of rf-magnetron sputtered In2O3 : Sn.* Solid State Ionics, 2004. 173(1-4): p. 141-145.

16. Roncali, J., *Conjugated Poly(Thiophenes) - Synthesis, Functionalization, and Applications.* Chemical Reviews, 1992. 92(4): p. 711-738.

17. Bokman, F., *Analytical Aspects of Atmospheric Pressure Ionization in Mass Spectrometry*. 2002.

18. Gilbert, W., *De Magnete*. 1600, Londini.

19. Bose, G.M., *Recherches Sur La Cause Et Sur La Veritable Theorie De L'Electricite*. 1745, Wittembergae.

20. Nollet, J.A., *Recherches Sur Les Causes Particulieres Des Phenomenes Electrique*. 1753, Paris.

21. Taylor, G.I., Proceedings of the Royal Society in London A A280.

22. Whitehouse, C.M., et al., *Electrospray Interface for Liquid Chromatographs and Mass Spectrometers.* Analytical Chemistry, 1985. 57(3): p. 675-679.

23. Yamashita, M. and J.B. Fenn, *Electrospray Ion-Source - Another Variation on the Free-Jet Theme.* Journal of Physical Chemistry, 1984. 88(20): p. 4451-4459.

24. Alexandrov, M.L., et al., *Ion Extraction from Solutions at Atmospheric-Pressure - a Method of Mass-Spectrometric Analysis of Bioorganic Substances.* Doklady Akademii Nauk Sssr, 1984. 277(2): p. 379-383.

25. Bruins, A.P., T.R. Covey, and J.D. Henion, *Ion Spray Interface for Combined Liquid Chromatography/Atmospheric Pressure Ionization Mass-Spectrometry.* Analytical Chemistry, 1987. 59(22): p. 2642-2646.

26. Wong, S.F., C.K. Meng, and J.B. Fenn, *Multiple Charging in Electrospray Ionization of Poly(Ethylene Glycols).* Journal of Physical Chemistry, 1988. 92(2): p. 546-550.

27. Wilm, M. and M. Mann, *Analytical properties of the nanoelectrospray ion source.* Analytical Chemistry, 1996. 68(1): p. 1-8.

28. Smith, D.P.H., *The Electrohydrodynamic Atomization of Liquids.* Ieee Transactions on Industry Applications, 1986. 22(3): p. 527-535.

29. Dole, M., L.L. Mack, and R.L. Hines, *Molecular Beams of Macroions.* Journal of Chemical Physics, 1968. 49(5): p. 2240-&.

30. Thomson, B.A. and J.V. Iribarne, *Field-Induced Ion Evaporation from Liquid Surfaces at Atmospheric-Pressure.* Journal of Chemical Physics, 1979. 71(11): p. 4451-4463.

31. Einstein, A., *Generation and conversion of light with regard to a heuristic point of view.* Annalen Der Physik, 1905. 17(6): p. 132-148.

32. Hufner, S. 2003.

33. Gargagliano, *Characterization of L-cysteine Thin Films Via Photoemission Spectroscopy*. 2005: Tampa.

34. Beerbom, M.M., et al., *Direct comparison of photoemission spectroscopy and in situ Kelvin probe work function measurements on indium tin oxide films.* Journal of Electron Spectroscopy and Related Phenomena, 2006. 152(1-2): p. 12-17.

35. Kojima, I. and M. Kurahashi, *Application of Asymmetrical Gaussian Lorentzian Mixed-Function for X-Ray Photoelectron Curve Synthesis.* Journal of Electron Spectroscopy and Related Phenomena, 1987. 42(2): p. 177-181.

36. Schlaf, R., H. Murata, and Z.H. Kafafi, *Work function measurements on indium tin oxide films.* Journal of Electron Spectroscopy and Related Phenomena, 2001. 120(1-3): p. 149-154.

37. Dannetun, P., et al., *The Chemical and Electronic-Structure of the Interface between Aluminum and Polythiophene Semiconductors.* Journal of Chemical Physics, 1993. 99(1): p. 664-672.

38. Salaneck, W.R., et al., *Thermochromism in Poly(3-Hexylthiophene) in the Solid-State - a Spectroscopic Study of Temperature-Dependent Conformational Defects.* Journal of Chemical Physics, 1988. 89(8): p. 4613-4619.

39. Knupfer, M. and G. Paasch, *Origin of the interface dipole at interfaces between undoped organic semiconductors and metals.* Journal of Vacuum Science & Technology A, 2005. 23(4): p. 1072-1077.

40. Nambu, A., et al., *Film growth and X-ray induced chemical reactions of thiophene adsorbed on Au(111).* Surface Science, 2003. 530(1-2): p. 101-110.

41. Burgi, L., et al., *Close look at charge carrier injection in polymer field-effect transistors.* Journal of Applied Physics, 2003. 94(9): p. 6129-6137.

42. Wan, A., et al., *Impact of electrode contamination on the alpha-NPD/Au hole injection barrier.* Organic Electronics, 2005. 6(1): p. 47-54.

43. Chen, T.A., X.M. Wu, and R.D. Rieke, *Regiocontrolled Synthesis of Poly(3-Alkylthiophenes) Mediated by Rieke Zinc - Their Characterization and Solid-State Properties.* Journal of the American Chemical Society, 1995. 117(1): p. 233-244.

44. Fujimoto, H., et al., *Ultraviolet Photoemission-Study of Oligothiophenes - Pi-Band Evolution and Geometries.* Journal of Chemical Physics, 1990. 92(7): p. 4077-4092.

45. Schwieger, T., et al., *Electronic properties of interfaces between different sexithiophenes and gold.* Journal of Applied Physics, 2005. 97(12).

46. Lagel, B., et al., *Investigation of the poly[2-methoxy-5-(2 '-ethyl-hexyloxy)-1,4-phenylene vinylene]/indium tin oxide interface using photoemission spectroscopy.* Journal of Applied Physics, 2005. 98(2).

47. Lyon, J.E., et al., *Photoemission study of the poly(3-hexylthiophene)/Au interface.* Applied Physics Letters, 2006. 88(22).